QUANTITATIVE BIOSTRATIGRAPHIC ANALYSIS OF MIDDLE CRETACEOUS SEQUENCES IN THE BALTIMORE CANYON TROUGH, OFFSHORE MID ATLANTIC U.S. MARGIN

By

LESLIE MARGARET JORDAN

A thesis submitted to the

School of Graduate Studies

Rutgers, The State University of New Jersey

In partial fulfillment of the requirements

For the degree of

Master of Science

Graduate Program in Earth and Planetary Sciences

Written under the direction of

Kenneth G. Miller

_____

_____

_____

_____

New Brunswick, New Jersey

October 2019

ABSTRACT OF THE THESIS

QUANTITATIVE BIOSTRATIGRAPHIC ANALYSIS OF MIDDLE CRETACEOUS SEQUENCES IN THE BALTIMORE CANYON TROUGH, OFFSHORE MID ATLANTIC U.S. MARGIN

by Leslie Margaret Jordan

Thesis Director:
Kenneth G. Miller

I applied multiple quantitative biostratigraphic methods to Cretaceous sequences from the Baltimore Canyon Trough, which lies offshore of the Mid-Atlantic U.S. Here, 569 planktonic foraminifera, nannofossil, and palynological events spanning 25 wells were used to define assemblage and interval zones, as well as major paleoenvironmental changes in the Dawson Canyon, Logan Canyon (three sequences), and Missisauga Formations (two sequences). Further, the ages of the sequences defined by Miller et al. (2018) were temporally constrained based on chronostratigraphically significant biostratigraphic markers that were identified in our analyses. They are as follows: the Late Cenomanian Dcx sequence (*Rotalipora cushmani* and *R. greenhornensis* Zone), the early Cenomanian LC1 sequence, the late Albian LC2 sequence (*Braarudosphaera africana*, *Planomalina buxtorfi*, and *Spinidinium vestitum* Zone), the late Aptian LC3 sequence (*Cyclonephelium tabulatum* Zone), and the early Aptian to Barremian MISS (*Aptea anaphrissa, Pseudoceratium pelliferum,* and *Muderongia simplex* Zone). These six biozones are correlated with six strong seismic reflectors that can be traced across the basin. Together, these seismic and biostratigraphic interpretations can be used to evaluate

reservoir continuity, that helps assess the viability of the basin as an offshore carbon storage reservoir.

ACKNOWLEDGMENTS

I would like to profoundly thank Ken Miller for every moment of time and word of encouragement he has given me since I arrived at Rutgers. His kindness means more to me than I can express here. I would also like to thank the other members of my committee, Jim Browning and Greg Mountain, for their encouragement and patience.

I would like to thank John Schmelz and Kim Baldwin for the components that they contributed to this thesis, and their help and support in this whole process.

I would like to thank Pete McLaughlin and Moji KunleDare of the Delaware Geological Survey for their help with technical methods used in this study, and Lydia Cumming and her colleagues at Battelle who led the Mid Atlantic Offshore Carbon Storage Resource Assessment Project.

I would like to thank my fellow geology graduate students for making me feel welcome and at home, for offering personal and professional support, and for being wonderful friends.

Finally, I would like to thank my family, who have supported my dreams and my growth as a geologist and as a person.

Thank you all so much for sharing this journey with me.

DEDICATION

To my father, Ben Jordan

Gone but never forgotten

TABLE OF CONTENTS

ABSTRACT OF THE THESIS ii

ACKNOWLEDGEMENTS iv

DEDICATION v

LIST OF ILLUSTRATIONS viii

I. **Introduction** **1**

i. Background 2

ii. Litho- and Sequence Stratigraphy 3

II. **Methods** **6**

i. Overview 6

ii. Ranking and Scaling 7

iii. Graphic correlation 8

iv. Event parameters 9

v. Monte Carlo analysis 10

III. **Results** **12**

i. Ocean Anoxic event and the Late Cenomanian biostratigraphic package 14

ii. Middle to Late Cenomanian Unconformity 15

iii. Early Cenomanian biostratigraphic package 15

iv. Late Albian Unconformity 16

v. Albian biostratigraphic package 17

vi. Early to Middle Albian Unconformity 18

vii. Aptian biostratigraphic package 18

viii. Aptian Unconformity 19

ix. Early Aptian to Barremian biostratigraphic package 19

IV. **Discussion** **20**

V. **Conclusion** **24**

VI. **REFERENCES** **26**

VII. **FIGURE CAPTIONS** **32**

VIII. **FIGURES** **35**

IX. **APPENDICES** **52**

i. Appendix A 52

ii. Appendix B 56

LIST OF ILLUSTRATIONS

Figure 1. Map of Baltimore Canyon Trough illustrating the area of the basin and the placement of drilled wells

Figure 2. Seismic profile for B-01-75- AT line 125A with traced reflectors and COST B2 gamma log

Figure 3. Correlation table showing the relationship between seismic reflectors, sequences, lithology, and biostratigraphic zones.

Figure 4. Fence diagram of wells from figure 3 with biostratigraphic event ties between each well

Figure 5. Gamma log survey records from dip transect wells with plotted sequences and biostratigraphic event

Figure 6. Age-depth plot for wells in dip transect and their respective RASC outputs

Figure 7. Geologic timescale with events from BCTCSS and dip transect wells

Figure 8. Dendrogram results from RASC analysis

Figure 9. Plotted variance analyses from RASC analysis

Figure 10. Age depth diagram of graphically correlated events

Figure 11. Plot of BCTCSS calculated relative depths

Figure 12. Major sequence stratigraphic, biostratigraphic, paleoenvironmental, and sea-level events for this study shown in relation to the geologic timescale

Figure 13. Range chart for bio- and sequence stratigraphic events

Figure 14. Results of the Monte Carlo simulation and estimated sedimentation rate

I. INTRODUCTION

Biostratigraphy is an essential tool in evaluating chronology and placing sequences into a chronologic framework (e.g., Aubry, 1995). The use of biostratigraphic data is critical to improving the resolution of mappable units in offshore oil and gas reservoirs. Inconstancies in the biostratigraphic record, such as incomplete sampling and variation in the distribution of taxa, can be identified by comparing records from different wells to a generated composite standard section. Unfortunately, these inconsistencies are varying and abundant, and can be classified as geological or methodological. Geologic problems include the quality of preservation in the rock record and variation in the distribution of fossil taxa including differing first and last appearances, while methodological problems include incomplete sampling and inconstant identification of the same species.

Microfossils are sensitive to sedimentation and depositional environment, that affect their preservation and occurrence in the rock record (e.g., Brett, 1995). These geologic processes include the presence of unconformities and associated hiatuses related to sea-level change and other processes. The ranges of calcareous nannofossil and planktonic foraminifera groups typically provide better age constraints than dinoflagellate cysts and pollen and spores, as evidenced in "global" biozones such as that of Ogg and Hinnov (2012). Biozones tend to be broad (1-4 myr), but even these broad biozones are important as they provide a framework for regional-scale, higher-resolution divisions. However, site specific biozones often differ due diachrony among locations, preservation quality, and regional paleoclimate events, all of which potentially affect the first and/or

last appearance ages. This is why it is essential to evaluate biostratigraphy on a regional or even basin wide scale.

Extensive work has been done by the oil and gas industry to identify and evaluate microfossil data in order to establish regional biozones. Industry wells from this study provided abundant data in the form of cuttings, which are rock samples collected from drilling fluid. Continental Offshore Stratigraphic Test (COST) wells collected additional 2-inch rotary sidewall cores. Both well types used a sampling interval of 30 feet (~10 meters) that limits resolution of biostratigraphic studies. Further, taxonomic understanding of the same species by different biostratigraphers can create additional inconstancies. Wells in the Baltimore Canyon Trough were operated by more than 5 companies, each with their own biostratigraphy team or contractor. Thus, more than a dozen different researchers worked on these reports, each with a potentially different understanding and ability to classify taxa.

This study aims to use quantitative biostratigraphic methods to increase the resolution of biostratigraphic interpretations of Cretaceous strata from the Baltimore Canyon Trough. I will assess the reliability of industry data in order to create correlative Cretaceous biozones that are consistent throughout this basin that can be used to enhance the accuracy of sequence and seismic stratigraphic analyses.

i. Background

The Baltimore Canyon Trough is a basin located offshore of New Jersey, U.S.A., that contains the thickest depocenter of post-rift sediments on the U.S. Atlantic continental margin (Fig. 1). It overlies a series of Mesozoic rift basins and a post-rift

unconformity that trend along eastern North America. This basin formed following the rifting of the North American and African plates in the Late Triassic to earliest Jurassic (Withjack et al., 1998). Syn-rift deposits consist of Appalachian clastic materials deposited by both fluvial and lacustrine systems and Central Atlantic Magmatic Province basalts and diabases (Poag, 1985; Sheridan et al., 1991). These units are separated from post-rift sediments by the post rift unconformity that represents the deepest mappable unconformity in the basin (Grow et al., 1988). Post-rift sedimentation is evidenced with the emplacement of fringing, progradational carbonates that created a stratigraphic shelf edge reef. These Upper Jurassic to lowermost Cretaceous reefal units are primarily interbedded oolitic grainstones and coral boundstones (Prather, 1991; Libby-French, 1984). The emplacement of the Great Stone Dome (GSD, sometimes termed the Schlee Dome) during the Early Cretaceous was originally hoped to provide the largest structural trap for hydrocarbons in this basin. A swarm of igneous dikes associated with the GSD has a strong magnetic anomaly that indicates it originated in the mantle (Epstein and Clark, 2009). The ages of this and the immediately overlying Cretaceous siliciclastic units are poorly constrained due deformation of bedding and the scarcity microfossils in the interbedded igneous-sedimentary complex.

ii. Litho- and Sequence Stratigraphy

The relationship between microfossil assemblages, sequence stratigraphic events, and paleoenvironments can be used to enhance sequence stratigraphic interpretations of previous studies (Fig. 3). Sequence boundaries are regional surfaces of erosion and/or nondeposition, as defined by Mitchum et al. (1977) that can be objectively recognized

with seismic, outcrop, and chronostratigraphic data. The incorporation of biostratigraphic data assists in differentiating between previously identified sequence stratigraphic packages, as well as providing age control. This study seeks to utilize this relationship with data from the Baltimore Canyon Trough.

This study focuses on post-rift Cretaceous deposits. These packages of strata have been the focus of studies seeking to characterize laterally continuous sand units that have been targets for hydrocarbon production (Libby-French, 1985; Prather, 1991; Brown et al., 2011) and more recently for carbon storage injection (Miller et al., 2017; 2018). Initial industry studies defined these units lithologically, but the recent release of seismic surveys and gamma logs enabled academics to define these units using sequence stratigraphy, and to evaluate changes in sea level and paleoenvironment (Miller et al., 2018; Schmelz et al., in press; Baldwin et al., submitted). Units in the Baltimore Canyon Trough follow the naming convention of the Scotian Shelf that are lithologically similar to this and other proximal basins (Libby-French, 1984). The units studied here are, in ascending order, the Missisauga, Logan Canyon, and Dawson Canyon Formations (Fig. 2). These lithologically defined units correspond to the sequence stratigraphic units MS, LC, and DCx (Miller et al., 2018).

The Missisauga Formation is predominately composed of thick, light gray heterolithic sandstones that are interbedded with black shales and limestone layers (Poag, 1985). These shales contain abundant terrestrial palynomorphs, as well as a few planktonic foraminifera and nannofossils. The biotic assemblage and lithology indicate

predominantly deltaic plain, delta front, or inner sublittoral depositional environments. It is separated from overlying units by the seismic reflector LK1 (Schmelz et al., 2019).

The Logan Canyon Formation has been split into three seismically and lithologically distinct sequences: LC3, LC2, and LC1 (Miller et al., 2018). LC3, the oldest sequence, is characterized by predominantly calcareous, porous sandstones and sandy, calcareous shales, interbedded with siltstone beds, and sparse coal beds (Poag, 1985). These lithological features suggest a tidally influenced depositional environment in the vicinity of the GSD and COST B2 well. Shell fragments and microgastropods in this shale layer, combined with the presence of terrestrial palynomorphs and dinoflagellate cysts, indicate an interdistributary bay to marginal marine and shelf environment. It is separated from younger Logan Canyon units by the seismic reflector MK3. The overlying LC2 sequence is characterized by thick, coarser grained sandstone beds. These sands were most likely deposited by channels and mouth bars, and indicate a non-marine to marginal marine paleoenvironment. Abundant terrestrial palynomorphs combined with few foraminifera support the conclusion of a paralic depositional environment. The Logan Canyon 2 sequence is separated from LC1 by the reflector MK2. The LC1 sequence is associated with marly to glauconitic shales and blocky sandstones (Poag, 1985). These shales are seen most prominently in COST B2, Conoco 590-1, and other distal wells, but are less distinct in wells most proximal to shore, including the GSD wells (Baldwin et al., submitted). Similar to LC1, LC2 lithologies represent shelf, delta front, and delta plain environments.

The Dawson Canyon Formation lies directly above the LC1 sequence, and is defined as the shales overlying the MK1 seismic reflector. These calcareous mudstone

units represent a major marine transgression. This formation encompasses the Cenomanian-Turonian boundary event (Ocean Anoxic Event 2) that is recognized as a gamma log high that lies above this first Cenomanian parasequence (Sugarman et al., 1999).

These lithologies and sequences are critical to understanding the evolutionary history of the Baltimore Canyon Trough. By adding biostratigraphic constraints to these data, we are able constrain the ages of these features. Further, microfossil data can serve as a control for paleoenvironment and systems tract interpretations. Facies shifts can be identified through changes in the microfossil assemblages. For example, species FADs and LADs are often clustered above sequence boundaries and at maximum flooding surfaces (MFS) (Brett, 1995). This clustering can be used to identify major unconformities and MFS. It is important to note that apparent ranges of taxa may vary within a basin and require secondary controls on the validity of the microfossil data. The control on the biostratigraphic data in this study is the use of quantitative methods. Both probabilistic and deterministic methods are used to recognize biostratigraphic zones in these identified sequences in Baltimore Canyon Trough.

II. METHODS

i. Overview

Exploration of the Baltimore Canyon Trough was two pronged: one by industry (1975–1983) of predominantly Jurassic- mid Cretaceous strata and one by scientific ocean drilling (1983–2009) of predominantly Miocene strata. Acquisition of seismic and

downhole data, as well as inhouse analyses, came from well completion reports released by BOEM and used in a U.S. Department of Energy study of the mid-Atlantic U.S. offshore carbon storage resource assessment. These wells include two continental offshore stratigraphic test (COST) wells and 23 industry wells from areas in Wilmington Canyon, Hudson Canyon, and Baltimore Rise (Fig. 1). Biostratigraphic samples were mostly taken from sidewall cores and ditch cuttings, with reports recording the highest common occurrence (HCO) of a species. This study uses 277 of 569 microfossil HCO events in 25 wells in the Baltimore Canyon Trough. Conventional petroleum exploration biozonal schemes are done by hand, which creates a lack of reproducibility and can lead to problems with high resolution correlations of zonal events (Gradstein et al., 1999). Here, microfossil data are reinterpreted using quantitative correlation techniques to improve resolution and its correlative potential among wells in this basin. This is done using graphic correlation and ranking and scaling methods.

ii. Ranking and Scaling

The ranking and scaling (RASC) method is useful in analyzing large datasets to constrain inconsistences between fossil events (Fig. 4). This probabilistic method of quantitative biostratigraphy was developed by Agterberg and Gradstein (1999). Ranking is used to create an optimum succession of events in relative time, and is used to overcome possible stratigraphic inconsistencies such as reworking, caving, or missing information. This is done using the Hay optimum sequence method, where ranking is based on the superpositional relationship between events (Agterberg and Gradstein, 1999). A stratigraphic inconsistency is defined as when an event is observed above

another event in some sections and below it in others. The RASC method resolves these inconsistencies by calculating crossover frequencies, and is defined as follows: if two events (A and B) co-occur in *n* sections with A above B in *n*(AB) sections, A below B in *n*(BA) sections, and A with B in the same sample in *n*(A-B) sections, then the crossover frequency of A with respect to B is $f(AB) = \{n(AB) + 0.5n(A\text{-}B)\}/n$. This means that two events that are coeval have crossover frequency equal to 0.5, and an event that occurs above another event in all sections has a crossover frequency of 1. A modified Hays method is used to resolve stratigraphic inconsistencies that involve more than two taxa. This modified Hays method utilizes presorting, where every event is compared with all other events before the calculation of crossover frequencies. If an event occurs more frequently above another event, it receives an additional score of +1; if it occurs more frequently below the other event its score is not increased; if it is coeval on the average with another event, both event scores are increased by 0.5 (Agterberg and Gradstein, 1999). An optimum sequence is determined by ordering events according to the magnitude of their total scores.

ii. Graphic correlation

Graphic correlation is a deterministic method of quantitative biostratigraphy first introduced in Shaw (1984). A two-axis graph is used to express time equivalence between stratigraphic sections in this method. First, a reference section must be selected (Edwards, 1984). This should be the most complete section, i.e. a well-sampled and unfaulted section containing many species at many levels. This is plotted on the x-axis, while the section it is being compared to is plotted on the y-axis.

The COST B2 well was selected as the reference section, as it has been considered a "Rosetta Stone" for the Baltimore Canyon Trough due to its extensive study and relatively complete logs (Miller et al., 2018). The location of time equivalent levels within pairs of sections are used to find the line of correlation (LOC) between the two wells. This line of correlation must have a positive slope, as time progresses in the positive direction. Several methods can be employed to find the LOC, including a straight linear ordinary least squares method, a straight linear reduced major axis regression, and piecewise linear. These mathematical techniques can be employed on all or select points. Shaw's original work used all points for analysis, though some argue that an expert's judgment regarding the relative value of different taxa and other stratigraphic information should be used in the analyses (Edwards, 1984). This study employs all points, and uses a straight linear reduced major axis regression to find the LOC. Once this line is drawn, a composite section is created. For more than two wells, data from the composite section are compared to a third section, which is used to create another composite section, and so on. Between three and six cycles of interpretation are required for fossil ranges of the composite section to become stable, thus indicating the best model.

iii. Event Parameters

Data points were extracted from 35 individual biostratigraphy reports for wells in the Baltimore Canyon Trough, totaling 569 events (Amato, 1978; Bifano, 1978; Callender, 1978; Crane, 1979a-c, 1982; Cousmeiner, 1986; Edelman, 1979; Edson, 1986, 1988; Exxon, 1980; Fairchild, 1979; Gauger, 1978; International Biostratigraphers Incorperated, 1978a-b, 1979a-d, 1980; Millioud, 1979; Scholle, 1977, 1980; Stapleton,

1981; Steinkraus 1979, 1985a-b; Stough 1978, 1979a-b, 1981a-b). This study defines an event as the highest common occurrence (HCO) of a fossil identified in a well. Microfossil groups from these original reports include benthic and planktonic foraminifera, dinoflagellate cysts, nannofossil, pollen, spores, and ostracods. Quantitative analyses in this study excluded ostracods and benthic foraminifera, as they are generally facies dependent groups. Species with synonymous names were consolidated into the naming convention more commonly used (i.e., *Globigerinelloides breggiensis* in well Exxon 684-2 and *Ticinella breggiensis* in well Tenneco 684-2 become *Biticinella breggiensis*, as in Exxon 500-1 and is the current accepted nomenclature). After setting these constraints, the number of bioevents decreased to 277. These events were used to perform the graphic correlation. When analyzing a dataset using ranking and scaling, parameters must be set for events in order to achieve the most useful output. The statistical parameter *k* is the minimum number of wells that a bioevent must occur in. This parameter creates stratigraphic constraints, as the total number of bioevents in the optimum sequence decreases with increasing *k* values (Gradstein et al., 2008). RASC analysis in this study used k=4, which decreased the total number of events to 179. These events were used to perform the ranking and scaling analysis.

iv. Monte Carlo analysis

A Monte Carlo analysis was done to supplement the graphic correlation results and to more accurately understand changes in sedimentation rate through time. Here, depth in CSU versus age was regressed for this analysis. This model uses computational methods to repeatedly randomly sample events to constrain the ranges of results. Here, the position of age for each individual taxa with a known range was changed, totaling

5000 runs. For each run, each taxon is randomly assigned age within known ranges. Ages assigned by the model follow a normal distribution centered around the midpoint of the total range, 95% of age estimates for a taxa are within the observed range of each species, allowing for 5% of individuals to exceed the current known ranges. This accounts for diachrony for the sample location. Each iteration of the model has a randomly assigned age for each taxa. A LOESS (LOcally Estimated Scatter plot Smoothing) regression is applied to each subset of ages produced by the Monte Carlo regression. This allows for a more precise age estimate to be constrained from the variable ranges of total known ages of each species, which is what was used to construct the composite standard section through graphic correlation. Any individual model runs that resulted in a negative sedimentation rate were rejected. Once LOESS regression is applied to each iteration, the average age for each depth in 100 ft intervals is calculated. The search window for the LOESS regression is 10000 CSU with an exponential decay, due to the sparsity of the data. The variability of these age estimates is bounded by the 95^{th} percentile (1.96 SD) of regression results at each GC depth. The mean of all regression results is shown in black. Sedimentation rate was estimated using this mean, and the median of the sedimentation rate is displayed similarly bound by lines that encompasses 95% of all results. This allows for a comparison to isopach models proposed by Schmelz et al. (submitted) and Baldwin et al. (submitted). This model provides quantifiable certainty to graphic correlation.

III. RESULTS

I observe major differences and contradictory results for a subset of our data in a data rich dip transect comprised of four wells, COST B2, Exxon 684-1, Texaco 598-1, and Tenneco 642-1, from probabilistic versus deterministic methods (Fig. 5). I compare results from graphic correlation and RASC methods. First, age-depth plots were made using existing data, without the assistance of quantitative methodologies (Fig. 6). The line of correlation in these diagrams intersects the ranges of *R. greenhornensis, P. buxtorfi*, *C. tabulatum*, and *M. simplex*, that are used as common anchor points for age-depth diagrams of all wells. These same points were used to determine the placement of the line of correlation when an age-depth plot was made using the FADs of taxa analyzed with graphic correlation methods. Then, this Baltimore Canyon Trough composite standard section (BCTCSS) was compared to the age-depth plots from wells in the dip transect (Fig. 7). Lastly, the 16 taxa that had high enough k values to be included in a RASC analysis were plotted using their RASC calculated depth in each well in their rank from youngest to oldest (Fig. 8). By comparing these different methods (traditional biostratigraphy, graphic correlation, and ranking and scaling) in the same four wells, we were able to determine the most effective method for our data.

RASC methods have been proven effective in a myriad of studies, particularly in Gradstein et al. (1999), that used the method to parse biozones from industry data in Cretaceous records from Norwegian offshore drilling. This method was unfortunately ineffective at untangling the biostratigraphic data from the Baltimore Canyon Trough. The primary difference in these studies was the resolution of data. Only 16 points had a

high enough k value to be included in the final, edited dataset. Of these 16 points, only 60 percent of these points were resolved with a standard deviation less than the mean (Fig. 9). This means that only 9 species were deemed statistically useful for creating biostratigraphic zones, which is insufficient when considering the more than 3000 feet (~1 km) of sediments that need to be characterized in the basin. RASC relative ages for taxa used violate known biostratigraphic ranges. Lastly, plotting the ranked sequence of events with a line of correlation shows a weak association of these RASC points to the LOC. There was also no evidence of major unconformities or stratigraphic changes in the RASC section, which was unhelpful in correlating biostratigraphic events to sequence stratigraphic packages. Graphic correlation provides a much more parsimonious solution compared to that of RASC, and provides a way to identify and date major sequence stratigraphic events.

Graphic correlation proved to be a more effective method for characterizing the Baltimore Canyon Trough, primarily because it included many more bioevents. Many more taxa were included in this analysis, as deterministic methods do not require such severe data editing. This yielded a composite standard section, which allowed us to estimate the approximate age of the HCO of more than 30 events that are associated with the intersection of the line of correlation used in age-depth plots for individual wells (Fig. 10). Further, plotting the calculated FAD points of the composite standard section provided unambiguous evidence for unconformities in the basin, that are interpreted here as sequence boundaries and MFS (Fig. 11). These unconformities are identified by horizontal slopes or data terraces, that are related to missing sections, low sedimentation, or hiatuses. Here, they are interpreted major depositional sequence boundaries. An

additional data terrace was identified between MK2 and MK3. This event is the MFS in the Logan Canyon 2 sequence. The overall quality of results of the graphic correlation were more fruitful in terms of included taxa and correlation to sequence stratigraphic events. This is why I have based my chronology on the composite standard sequence created using this method (Fig. 12). Here we develop a chronology of sequences and events and discuss them from youngest to oldest.

i. Ocean Anoxic event and the Late Cenomanian biostratigraphic package

The top of the studied interval is the Cenomanian Turonian Boundary Event (Fig. 10), here referred to as Ocean Anoxic Event 2 (OAE2). This event is identified in the rock record by organic-rich black shale with positive large carbon isotope excursions (Jenkyns, 2010; Wright et al., 2001; Alexandre et al., 2010). These deposits are also strongly enriched in uranium and other trace metals that can serve as a proxy for total organic carbon (Luning and Kolonic, 2003). Therefore, the level of OAE2 in the wells of the Baltimore Canyon Trough can be approximated using gamma log highs from well logs. This event is temporally constrained by its occurrence in the DCx sequence and its occurrence above the HO of *Rotalipora cushmani*. This OAE was similarly identified on the New Jersey Coastal Plain in the ODP 174AX Bass River core (Sugarman et al., 1999). This planktonic foraminifer is the most consistent and significant bioevent reported, as it occurs in 18 out of 22 wells. It was used by Miller et al. (2018) to differentiate between shales of Dawson Canyon and the upper Logan Canyon sequence that had previously been miscorrelated by Libby-French (1984). *Rotalipora greenhornensis* is also confined solely within the DCx sequence. The presence of these

two species indicate that this sequence is late Cenomanian. This sequence also has the highest calculated sedimentation rate of all Cretaceous sequences assessed. Micropaleontological assemblages from this interval are characterized by these rotaliporid planktonic foraminifera, which suggests a middle to outer sublittoral paleoenvironment.

ii. Middle to Late Cenomanian Unconformity

Sequences DCx and LC1 are separated by the MK1 reflector. This sequence boundary is equivalent to the major mid-Cenomanian unconformity identified by Vail et al. (1980). This unconformity is considered "global" in extent, as the result of a major sea-level fall (Haq, 2014). This sea-level event had previously been identified onshore New Jersey by Miller et al. (2003, 2005). Major unconformities such as this are most easily recognized using seismic data; it has been defined as reflector MK1 in seismic studies of Baltimore Canyon Trough (Miller et al., 2018; Schmelz et al., in press; Baldwin et al., submitted). The highest occurrences of *R. greenhornensis* and/or *R. appenenica*, and *Praeglobotruncana stephani* in COST B2, Tenneco 642-2, Homco 676-1, Homco 855-1, Exxon 500-1, and Gulf 718-1 were used to determine the presence of this hiatus that occurred from approximately 96.2-95 Ma.

iii. Early Cenomanian biostratigraphic package

This Logan Canyon 1 (LC1) sequence is defined by the absence of well-defined, Cenomanian microfossils bracketed by the MK1 and bold MK2 seismic reflectors. This unit is composed of sandy, non-marine strata in wells more proximal to shore and pinches

out to a marine mudstone in more distal southeastern wells. The paleoenvironment inferred from these lithologies is a wave-dominated delta, with the coarser sands representing prograding mouth bar sands and shales representing a destructional phase of the delta (Libby-French, 1984). Wells exhibiting more of the sandy lithology in the LC1 sequence include Exxon 500-1, Mobil 544-1, Homco 676-1, Gulf 718-1, and Conoco 590-1. Down dip wells show a dramatically thinned truncated (<100 m), shale dominated sequence (Baldwin et al., submitted). Micropaleontological assemblages are generally poor, with many of the taxa reworked from the underlying LC2 sequence package.

iv. Late Albian Unconformity

The MK2 seismic sequence boundary correlates to the base of the LC1 sequence. It is also most likely correlated with the KAI8 sea level event of Haq (2014). This unconformity has been identified in the Baltimore Canyon Trough by the clustering of the first occurrences of species whose ranges are strictly older than middle to late Albian (i.e., palynomorph *Klukisporites pseudoreticulatus*) just below species whose ranges are limited to the Cenomanian to early Albian (i.e., foraminifer *Planomalina buxtorfi)*. An apparently coeval unconformity was similarly identified using biostratigraphic markers on the Scotian shelf by Weston et al. (2012). This late Albian event is interpreted as a progradational truncation event, which can be identified on seismic surveys in the Baltimore Canyon Trough (Schmelz et. al, in press), Georges Bank Basin (Adams, 2019), and the Scotian Shelf (Weston et. al, 2012). Well log analyses also evidence this late Albian unconformity through sharply contrasted blocky sands of the LC2 sequence and

Cenomanian shales of the LC1 sequence (Miller et. al, 2018). This hiatus is estimated to occur from 101.2-98.7 Ma (Fig. 7).

v. Albian biostratigraphic package

This interval, that corresponds to the LC2 sequence, has the highest number of biostratigraphic events of all intervals analyzed. The younger cluster of this biostratigraphic package best correspond to the palynologic *Coronatispora valdensis-Trilobosporites humilis* assemblage-Zone of Bebout (1981), while the lower cluster best represents the *Auritulinasporites deltaformis-Cerebropollenites mesozoicus* assemblage Zone. This biostratigraphic package shows an increase in nannofossils in the beginning of this interval, as evidenced by the HO of *Corollithion signum "A", Podorhabdus albianus*, and *Braarudosphaera africana* above the MK2 sequence boundary and hiatus. Other species that characterize the late Albian part of this zone are the planktonic foraminifera *Hedbergella simplex*, *H. washitensis*, *Planomania buxtorfi*, *Biticinella breggiensis*, and *Praeglobotruncana turbinata*. The HO of *P. buxtorfi* is used to define this LC2 sequence in the majority of the wells in BCT, as noted by Miller et al. (2018). Dinoflagellate cysts *Apteodinium grande* and *Lithosphaeridium siphoniphorum* are also used to recognize the middle to late Albian. This primarily nannofossil and planktonic foraminifera assemblage indicates a sublittoral paleoenvironment. This Albian biostratigraphic package is similarly recognized on the Scotian Shelf, where *A. grande* and *R. rugosus* identify a middle Albian unconformity (Weston et al., 2012). A lithological and biostratigraphic transition occurred in the early Albian, with a facies shift from a transgressive systems tracts (TST) to a highstand systems tract (HST) (Schmelz et al., in press). This change is

evident in the Scotian Shelf through the shift from Logan Canyon sands to Naskapi shales. This change is also observed in the Baltimore Canyon Trough through a change from transgressive systems tract calcareous shales and sandstone to pyritic red and gray shales and coal (Scholle, 1977). This is observed in the biostratigraphic record by a shift from nannofossil and planktonic foraminifera-dominated assemblage to a dinoflagellate- and palynological-dominated assemblage.

vi. Early to Middle Albian Unconformity

The unconformity that delineates the bottom of the Logan Canyon 2 sequence and biostratigraphic zone is equivalent to the MK3 seismic reflector. The hiatus associated with the unconformity lasted from the early to middle Albian, roughly 113.9-107.6 Ma (Fig. 7). The length of this hiatus is based on the cluster HO of palynomorph species *Concavissimisporites punctatus*, *Pilosisporites trichopapillosus*, *Corollina torosa*, and *Rugbivesiculites rugosus*. This hiatus is bounded by the KAl3 and KAp7 events that represent sea-level falls and cycle boundaries (Haq, 2014). These global sea-level changes correspond with the shift from marine dominated to tidally influenced and non marine biofacies.

vii. Aptian biostratigraphic package

Cyclonephelium tabulatum is the most prominent biostratigraphic marker correlated to in the Aptian Logan Canyon 3 sequence. Biostratigraphic markers in this interval come from shale beds that roughly correlate to the Naskapi Shale of the Scotian Shelf. Nannofossil *Nannoconus globulus* and dinoflagellate *Canningia colliveri* temporally constrain the top of this section to the latest Aptian. The presence of

nannofossils (including *N. globulus* and *C. margereli*) indicate that the depositional environment of these shales is shallow marine. The shale layers that comprise the upper half of the section contain the marker taxa for this interval. Lower sand bodies are calcareous, fine-medium grained sandstones that show no biostratigraphic markers. This change in lithology and paleoenvironment represents a facies shift from a lowstand systems tract defined by terrestrial palynomorphs to a TST and HST defined by foraminifera and nannofossils (Schmelz et al., in press; Baldwin et al., submitted).

viii. Aptian unconformity

The unconformity that correlates to the basal LK1 seismic sequence boundary constrains the bottom of the Aptian biostratigraphic zone, which lasts from roughly 125-120 Ma (Fig. 7). The highest occurrence of dinoflagellate *Aptea anaphrissa* is used to identify this unconformity and hiatus. This likely corresponds with sea-level event KAp3 (Haq, 2014).

ix. Early Aptian to Barremian biostratigraphic package

The Barremian biostratigraphic package is equivalent to the MISS sequence in the Baltimore Canyon Trough, that likely contains at least two sequences (Baldwin et al, submitted; Schmelz et al., in press). The biotic assemblage in these sediments is exclusively composed of dinoflagellates and other palynomorphs. Age deterministic biostratigraphic markers include *Canningia attadalica*, *Cicatricosisporites australiensis*, *Pseudoceratium pelliferum*, and *Astrocysta cretacea*. This corresponds to the

Callialasporites sp. 4- *Cicatricosisporites australiensis* palynologic assemblage zone of Bebout (1981).

OAE 1a is an early Aptian (126-124 Ma) isotope excursion that is characterized by enhanced organic matter burial and the large-scale deposition of black shales, that was followed by a positive excursion in $\delta^{13}C$ values. Evidence of this global scale anoxic event is found in the Baltimore Canyon Trough. Total organic carbon (TOC) studies in the COST B2 well indicate shale beds and a TOC high at 9700 ft (~2960 m). Geochemical analyses of COST B2 cores place the carbon isotope excursion at 9500 ft (~2900 m) (Scholle, 1977). This places OAE1a at the first shaley interval under the sequence boundary LK1 in the COST B2 well, near the top of the Missisauga Formation. This formation is typically heterolithic and sand-prone (Baldwin et al., submitted). This sequence has the most variability in terms of sedimentation rate. The emplacement of the GSD constrains the base of this biostratigraphic analysis, as the intrusion of this igneous body caused a structural unconformity in the middle Barremian (Amato and Giordano, 1985; Baldwin et al., submitted).

IV. DISCUSSION

The biostratigraphic trends analyzed in this study of the Baltimore Canyon Trough provide age constraints for stratigraphic sequences of the Cretaceous that had been previously analyzed (Miller et al., 2017; Miller et al., 2018; Schmelz et al., in press; Baldwin et al., submitted) (Fig. 13). These studies used seismic profiles and gamma logs

to define sequence boundaries MK1, MK2, MK3, and LK1 in middle Cretaceous sand and shale units. These sequences provide a framework for which paleontological information can be examined. Data obtained from industry and scientific drilling in this basin provided enough biostratigraphic events to create a composite standard section, that can be used to constrain depositional ages of sequence packages, constrain the duration of sequence boundaries, and enhance the understanding of the paleoenvironment.

A composite standard section (CSS) was generated for this study using graphic correlation (Fig. 13). This deterministic method of quantitative biostratigraphy yielded the most realistic composite standard, that serves as a structure into which all bio and seismic events can be incorporated. A Monte Carlo analysis of this CSS was run to check this method (Fig. 14). Results of this analyses confirmed the ages of the hiatuses observed, and assisted in making comparisons of sedimentation rates between the sequences. Weston et al. (2012) defined sequence boundaries and biostratigraphic packages for the stratigraphically equivalent interval on the Scotian Shelf using palynology (including dinoflagellate cysts), foraminifera, and nannofossils. However, major differences in deposition, including sedimentation rate, and regional climate makes it necessary to develop a basin-specific composite section rather than rely on one that most likely similar but not study area specific. Further, the graphic correlation method is ideal for identifying and quantifying hiatuses that are evident in horizontal discontinuities. The CSS from the Baltimore Canyon Trough (BCTCSS) can also be used to determine the highest common well occurrences of identified species.

A main objective of this study was to identify regionally chronostratigraphically important taxa for each of these middle Cretaceous sequences. These are defined here as

taxa that appear in only one sequence in multiple wells. Previously, biostratigraphic markers were chosen based only on the HO of key marker taxa in a given well, including only the following: *Rotalipora cushmani, Spinidium vestitum, Cyclonephelium tabulatum, Muderongia simplex, Rotalipora appenninica, Planomalina buxtorfi,* and *Biticinella breggiensis* (Miller et al., 2017; Baldwin et al., submitted). While perhaps useful in differentiating sequences with similar lithologies, this small number of taxa is insufficient for a robust biostratigraphic characterization of the studied time interval. Introducing the graphic correlation method to this dataset aids in identifying less frequent, but chronostratigraphically significant, taxa. The BCTCSS shows us the most likely succession confining specific taxon. Further, it is helpful in indicating if a sequence boundary has been placed too low or too high. For example, the Dawson Canyon sequence is characterized by the highest common occurrence of *Rotalipora cushmani* and *R. greenhornensis*. This unit is lithologically homogenous, and can make placing sequence boundaries difficult without biostratigraphic constraints.

Graphic correlation is also an ideal method for the BCT because it constrains the duration of hiatuses that were associated with sequence boundaries. BCTCSS were used to differentiate condensed sections from unconformities. The constant slopes of lines of correlation before and after data discontinuities indicates a condensed section hiatus while different slopes are indicative of an unconformity (Stein et al., 1995). Condensed sections are common in pelagic and hemipelagic sediments that have characteristically low sedimentation rates, and can be indicative of a MFS when analyzing sequence stratigraphy (Baraboshkin, 2009). By plotting FADs assigned by graphic correlation, we

identify an intra-Albian MFS in the LC2 sequence in addition to the Cretaceous sequences of Miller et al. (2018).

While automated to semi-automated methods of biostratigraphy are convenient for analyzing large data sets, they often come with errors that arise from lack of appropriate geological constraints that are necessary to create a reliable interpretation. The Ranking and Scaling (RASC) method developed by Agterberg and Gradstein (1999) is an almost fully automated quantitative biostratigraphic program that creates a probabilistic interpretation. This method was used on biostratigraphic data from Baltimore Canyon and yielded poor results. This is because purely statistical methods are inappropriate for creating correlations between wells when there is high crossover frequency between biostratigraphic markers that arises from lack of high-resolution data.

The graphic correlation method that allows the biostratigrapher to have input on correlations through the selection of the main points of correlation. This means that, when using the graphic correlation method, some points that more accurately represent time can be emphasized over others. These are often events that have a brief but precisely dated occurrence. For example, foraminifer *R. cushmani* (93.9-95.6 Ma) can be emphasized over the occurrence of the pollen *C. punctatus* (96.3-145 Ma). Graphic correlation allows the user to preferentially select one point over the other in their discretion, while both points are considered to have equal weight in RASC programs. This was one of the main failures of the RASC method when applied to the BCT dataset. Further, the relative spacing of events (i.e. HCO, OAEs, and sequence boundaries) in the graphic correlation CSS is derived from the original stratigraphic spacing, rather than based on calculated pairwise crossover frequencies as in RASC. It is important to

preserve these original stratigraphic relationships, as they yield information about the duration of hiatuses and timing of shifts in paleoenvironment. Successful studies of Cretaceous biostratigraphic packages have been published using RASC, but these datasets are much larger than the one used in this study. Gradstein et al. (1999) used more than 30 wells even after omitting wells that "suffer from poor data coverage". The average well in their study contained more than 50 events, while wells in BCT only contain between 9 (Shell 272-1) and 26 events (COST B2). Graphic correlation easily can accommodate this type of small, scattered dataset, while RASC is most efficient with more robust dataset. This is why the optimal quantitative method for this study was graphic correlation. The use of this to method create a composite standard section for the middle Cretaceous sequences of the Baltimore Canyon Trough has added mathematical rigor to the biostratigraphic interpretation, and has assisted in better constraining the placement and ages of sequence boundaries.

V. CONCLUSION

By creating a composite standard section of Baltimore Canyon Trough, I was able to further constrain the position of sequence boundaries and assign ages to sequences and unconformities originally proposed by Miller et al. (2018). Biostratigraphic packages that correspond to each of the major sequences were defined by chronostratigraphically significant taxa identified through the use of this quantitative method.

The Dawson Canyon sequence has been assigned an age of late Cenomanian due to the consistent occurrence of *Rotalipora cushmani* and *R. greenhornensis*. These

planktonic foraminifera also helped constrain the depth of OAE2 black shales within an interval that is composed of relatively homogenous shales. The LC1 sequence is defined by its lack of identifying taxa, with wells such as COST B2 subject to reworking in this interval. The LC2 and LC3 sequences can both have facies shifts that can be identified by changes in the biostratigraphy. HST in LC2 are characterized by nannofossil and foraminifera, particularly *Podorhabdus albianus*, *Braarudosphaera africana, Planomalina buxtorfi,* and *Biticinella breggiensis*. The shift from palynomorphs *Spinidinium vestitum*, *Concavissimisporites punctatus*, and *Rugubivesiculites rugosus* is evidence for a TST. The LC2 sequence has been assigned an age of middle to late Albian based on these taxa. A similar shift in facies is seen in the LC3 sequence, where the nannofossils *Nannoconus globulus* and *Cyclagelosphaera margereli* are present in the HST facies, and the absence of biostratigraphic markers in the lower part of the sequence indicate a TST. This sequence is early Aptian. Lastly, dinoflagellates *Muderongia simplex*, *Aptea anaphrissa*, and *Pseudoceratium pelliferum* define the nonmarine facies in the Missisauga sequence, and has been assigned an age of early Aptian to Barremian.

The integration of sequence stratigraphy, lithostratigraphy, and biostratigraphy allows for a higher resolution characterization of the Baltimore Canyon Trough basin, offshore New Jersey. The middle Cretaceous sands from this study are potential carbon storage target areas. The chronostratigraphically significant biostratigraphic markers for each of these units defined by this study will aid in future CO_2 injection projects. The laterally continuous sands and shales create ideal storage targets and confining units for this type of environmental remediation.

VI. REFERENCES

Adams, A.C. 2019. Seismic stratigraphy of the Georges Bank Basin: Implications for carbon sequestration. Master's dissertation, Rutgers University, 78 pp.

Alexandre, J.T., Tuenter, E., Henstra, G.A., van der Zwan, K.J., van de Wal, R.S., Dijkstra, H.A., Boer, P.L. 2010. The mid-Cretaceous North Atlantic nutrient trap: Black shales and OAEs. Paleoceanography, v. 25, PA4201.

Agterberg, F.P., Gradstein, F.M. 1999. The RASC method for ranking and scaling of biostratigraphic events. Earth-Science Reviews, v. 46, pp. 1-25.

Amato, R.V., Giordano, A.C. 1985. Great Stone Dome—Great Disappointment? Abstract. AAPG Eastern Section Meeting with Abstracts, v. 69(9), pp. 1433.

Aubry, M.P. 1995. From chronology to stratigraphy: Interpreting the Lower and Middle Eocene stratigraphic record in the Atlantic Ocean. Geochronology, time scales and global stratigraphic correlation, pp. 213-274.

Baraboshkin, E.Y. 2009. Condensed sections: Terminology, types, and accumulation conditions. Moscow University Geology Bulletin, v. 64(3), pp. 153-160.

Bebout, J.W. 1981. An informal palynologic zonation for the cretaceous system of the United States mid-Atlantic (Baltimore canyon area) outer continental shelf. Palynology, v. 5, pp. 159-194.

Bifano, F.V. 1978. Gulf Energy and Minerals block 857, Hudson Canyon, #1 OCS A-0059, Baltimore Canyon area. Unpublished report for well API #61-105-00008, Paleo-Data, Inc.

Brett, C.E. 1995. Sequence stratigraphy, biostratigraphy, and taphonomy in shallow marine environments. PALAIOS, v. 10, pp. 597-616.

Brown, A.L., Berlin, E.H., Butsch, R.J., Senel, O., Mills, J., Harichandran, A., Sclumberger Carbon Services, Wang, J., Schlumberger Data Consulting Services, 2011. Carbon capture and sequestration: ascertaining CO_2 storage potential, offshore New Jersey, USA, Offshore Technology Conference, OTC 21995.

Callender, A.D Jr. and Bakos, N.A. 1978. Foraminiferal, environmental and nannofossil summaries, Texaco #1 OCS-A-0028 federal block 598 offshore New Jersey. Unpublished report for well API #61-105-00004, International Biostratigraphers Incorporated.

Crane, M.J. 1979a. Paleontological Section, Exxon Hudson Canyon blk. 684, #2 OCS-A-0046, API 61105 00010. Unpublished report for well API #61-105-00010, Exxon Company, U.S.A., Gulf/Atlantic Division.

Crane, M. 1979b. Exxon 902-1 Exploratory Well Summary. Unpublished report from well API #61-105-00013, Exxon Company, U.S.A., Offshore/Alaska Division.

Crane, M.J. 1979c. Exploratory well summary, Exxon OCS-A-0009 No.1, North Mallard. Unpublished report for well API #61-105-00016, Exxon Company, U.S.A. Gulf/Atlantic Division.

Crane, M.J. 1982. Paleontologic Section, Exxon Hudson Canyon B/684, #1 OCS-A-0046, API 61-105-000020. Unpublished report for well API #61-105-00002, Exxon Company, U.S.A. Gulf/Atlantic Division.

Cousminer, H.L., Steinkraus, W., Hall, R. 1986. Paleontology: Exxon OCS-A 0029-1, Block 599-1. Unpublished report for well API #61-105-00019.

Edelman, D.W., Gauger, D.J., Percival, S.F., Thompson, L.B. 1979. Biostratigraphy, paleoecology, visual kerogen analysis, vitrinite reflectance studies, and hydrocarbon source-bed evaluation of the Mobil 17-2 well, Avalon area, offshore New Jersey. Unpublished report for well API #61-104-00005.

Edson, G.M., ed. 1986. Shell Wilmington Canyon 586-1 well, Geological and operational summary, OCS Report MMS 86-0099. U.S. Department of the Interior, Minerals Management Service, Atlantic OCS Region.

Edson, G.M. ed. 1988. Shell Wilmington Canyon 372-1 well, Geological and operational summary, OSC Report MMS 87-0118. U.S. Department of the Interior, Minerals Management Service, Atlantic OCS Region. Unpublished report for well API #61-1040-0011.

Epstein, S.A., Clark, D. 2009. Baltimore Canyon untested gas potential. Carbonates and Evaporites, v. 24(1), pp. 58-76.

Exxon Company, U.S.A. 1980. Microfossil summary, Exxon No.2 OCS-A-0046, NJ18-3 API 61105-10. Unpublished report for well API #61-105-00010.

Fairchild, W.W. 1979. Biostratigraphy of the Tenneco OCS-A-0038 No. 2 block 642 Well. Unpublished report for well API # 61-105-00014, International Biostratigraphers Incorporated.

Gauger, D.J., Griffith, C.E., Percival, S.F., Thompson, L.B. 1978. Preliminary biostratigraphy and vitrinite reflectance data of the Mobil 544-1a, Baltimore Canyon, Offshore, New Jersey (ESC Request No. 311643). Unpublished report for well API #61-105-00003.

Gradstein, F.M., Kaminski, M.A., Agterberg, F.P. 1999. Biostratigraphy and paleoceanography of the Cretaceous seaway between Norway and Greenland. Earth-Science Reviews, v. 46, pp. 27-98.

Grow, J.A., Klitgord K.D., Schlee, J.S. 1988. Structure and evolution of Baltimore Canyon trough in Sheridan, R.E., and Grow, J.A., eds., Continental Margin, U.S.: Geological Society of America, The Geology of North America, v. 1-2. Biostratigraphy and paleoceanography of the Cretaceous seaway between Norway and Greenland. Earth-Science Reviews, v. 46, pp. 27-98.

Hardenbol, J., Thierry, J., Farley, M. B., Jacquin, T.H., de Graciansky, P.C., Vail, P. R. 1999; Mesozoic and Cenozoic Sequence Chronostratigraphic Framework of European Basins. SEPM Special Publication 60, Publisher: SEPM, Tulsa, OK, pp. #3-29.

Haq, B. 2014. Cretaceous Eustasy Revisited. Global and Planetary Change, v. 113, pp. 44-58.

Hay, W.W. 1972. Probabilistic stratigraphy. Eclogae Geologicae Helvetiae #v. 65, pp. #255–266.

International Biostratigraphers Incorporated. 1978a. Palynology of the Texaco #1 OCS-A-0028 federal block 598 well. Unpublished report for well API # 61-105-00004.

International Biostratigraphers Incorporated. 1978b. Biostratigraphy of the Continental Oil OCS-A-0024 blk, 590 Hudson Canyon well #1. Unpublished report for well API #61-105-00007.

International Biostratigraphers Incorporated. 1979a. Biostratigraphy of the Houston Oil and Minerals OCS-A-0042 block 676 No.1 well. Unpublished report for well API #61-105-00006.

International Biostratigraphers Incorporated. 1979b. Biostratigraphy of the Tenneco OCS A-0131 block 495 No.1 well. Unpublished report for well API #61-104-00007.

International Biostratigraphers Incorporated. 1979c. Palynology of the Texaco #2 OCS-A-0028 federal block 598 well. Unpublished report for well API #61-105-00011.

International Biostratigraphers Incorporated. 1979d. Biostratigraphy of the Houston Oil and Minerals OCS-A-0057 block 855 No.1 well. Unpublished report for well API #61-105-00012.

International Biostratigraphers Incorporated. 1980. Biostratigraphy of the Murphy OCS A-0081 #1 federal block 106 well. Unpublished report for well API #61-104-00008.

Jenkyns, H.C. 2010. Geochemistry of ocean anoxic events. Geochemisty, Geophysics, and Geosystems, v. 11(3), 30 pgs.

Libby-French, J.1984. Stratigraphic framework and petroleum potential of northeastern Baltimore Canyon Trough, mid-Atlantic outer continental shelf. American Association of Petroleum Geologists Bulletin, v.68(1), pp. 50-73.

Luning, S. and Kolonic, S. 2003. Uranium spectral gamma-ray response as a proxy for organic richness in black shales: applicability and limitations. Journal of Petroleum Geology, v. 26, no. 2, pp. 153-174.

Miller, K.G., Browning, J.V., Sugarman, P.J., Monteverde, D.H., Andreasen, D.C., Lombardi, C., Thornburg, J., Fan, Y., Kopp, R.E., 2017. Lower to mid-Cretaceous sequence stratigraphy and characterization of CO_2 storage potential in the mid-Atlantic U.S. coastal plain. Journal of Sedimentary Research v. 87, pp. 609-629.

Miller, K.G., Lombardi, C.J., Browning, J.V., Schmelz, W.S., Gallegos, G., Mountain, G.S., Baldwin, K.E. 2018. Back to basics of sequence stratigraphy: early Miocene and mid-Cretaceous examples from the New Jersey paleoshelf. Journal of Sedimentary Research, v. #88, pp. 148-179.

Miller, K.G., Sugarman, P.J., Browning, J.V., et al., 2003. Late Cretaceous chronology of large, rapid sea-level changes: glacioeustasy during the greenhouse world. Geology, v. 31, pp. 585–588.

Miller, K.G., Kominz, M.A., Browning, J.V., et al., 2005. The Phanerozoic record of global sea-level change. Science 312, pp. 1293–1298.

Millioud, M.E. 1979. Palynological study of the Exxon Company U.S.A. P-1 well, Baltimore Canyon. Unpublished report for well API #61-105-00002, Exxon Production Research Company, Basin Exploration Division.

Mitchum, R.M., Vail, P.V., Sangree, J.B. 1977. Stratigraphic interpretation of seismic reflection patterns in depositional sequences. Seismic stratigraphy – applications to hydrocarbon exploration. American Association of Petroleum Geologists Memoir, v. 26, pp. 117-134.

Ogg, G.J., Hinnov, A.L. 2012. The Cretaceous Period. In: Gradstein et al., The Geologic Time Scale 2012. Elsevier Publishing.

Poag, C. W. 1985. Geologic evolution of the United States Atlantic margin. New York: Van Nostrand Reinhold.

Prather, B.E. 1991. Petroleum geology of the Upper Jurassic and Lower Cretaceous, Baltimore Canyon Trough, western North Atlantic Ocean. AAPG Bulletin, v. 75, no. 2, p. 258-277.

Scholle, P.A. ed. 1977. Geological studies on the COST No. B-2 well, U.S. Mid-Atlantic outer continental shelf, Circular 750, U.S. Geological Survey 10.3133/cir750.

Scholle, P.A. ed. 1980. Geological studies of the COST No. B-3 Well, United States Mid-Atlantic continental slope area. Circular 833, U.S. Geological Survey 10.3133/cir833.

Sheridan, R.E., Olsson, R.K., Miller, J.J. 1991. Seismic reflection and gravity study of proposed Taconic suture under the New Jersey Coastal Plain: implications for continental growth. Geological Society of America Bulletin, v. #103, pp. 402-414.

Stapleton, R.P., Abbott, W.H., Morin, R.W., Thompson, L.B. 1981. Biostratigraphy of Mobil block 544-2, Baltimore Canyon, offshore, New Jersey (ESC request No.311A91). Unpublished report for well API #61-105-00023.

Stein, J.A., Gamber, J.H., Krebs, W.N., La Coe, M.K. 1995. A composite standard approach to biostratigraphic evaluation of the North Sea Paleogene. Norwegian Petroleum Society Special Publications, v. 5, pp. 401-414.

Steinkraus, W.E. 1979. Paleontological Summary and Biostratigraphic Report. Unpublished report for well API #61-104-00001, Shell Oil Company, Southeastern Region, Offshore Exploration Division.

Steinkraus, W.E., Bebout, J., Fry, C., Bielak, L. 1985a. Paleontology, Shell OCS-A-0096, Block 272. R. Hall, ed. Unpublished report for well API #61-104-00003.

Steinkraus, W., Hall, R., Cousminer, H. 1985b. Gulf 718 Biostratigraphy report. Unpublished report for well API #61-105-00005.

Stough, J.B. 1978. Palynology of the Exxon OCS-A 0046 No.1 (Pintail Prospect), offshore New Jersey. Report number 78-41. Unpublished report for well API #61-105-00002, Exxon Company, U.S.A., Headquarters Paleontology Laboratory, Exploration Department.

Stough, J.B. 1979a. Palynology of the Exxon No. #1 OCS-A-0065, Hudson Canyon block 902 (Canvasback prospect). Report number 79-23. Unpublished report for well API #61-105-00013, Exxon Company, U.S.A., Headquarters Paleontology Laboratory, Exploration Department.

Stough, J.B. 1979b. Palynology of the Exxon OCS-A-0046 No.2 (Pintail prospect), offshore New Jersey. Report number 79-30. Unpublished report for well API #61-105-00010, Exxon Company, U.S.A., Headquarters Paleontology Laboratory, Exploration Department

Stough, J.B., Crane, M. 1981a. Paleontological section, Exxon Hudson Canyon B/816, #1 OCS-A-0055. Report number 81-14. Unpublished report for well API #61-105-00020, Exxon Company, U.S.A., Gulf/Atlantic Division.

Stough, J.B. 1981b. Palynology of the Exxon OCS-A-0052 No.1 block 728, South Pintail prospect, offshore New Jersey (Hudson Canyon). Report number 81-17. Unpublished report for well API #61-105-00022, Exxon Company, U.S.A., Headquarters Paleontology Laboratory, Exploration Department.

Sugarman, P.J., Miller, K.G., Olsson, R.K., Browning, J.V., Wright, J.D., De Romero, L.M., White, T.S., Muller, F.L., Uptegrove, J. 1999. The Cenomanian/Turonian carbon burial event, Bass River, NJ, USA: Geochemical, paleoecological, and sea-level changes. Journal of Foraminiferal Research, v. 29(4), p. 438-452.

Vail, P.R., Mitchum, R.M., Shipley, T.H., Buffler, R.T. 1980. Unconformities of the North Atlantic. Philosophical Transactions of the Royal Society A, v. 294, pp. 137-155.

Weston, J.F., MacRae, R.A, Ascoli, P., Kevin, M., Cooper, E., Fensome, R.A., Shaw, D., Williams, G.L. 2012. A revised biostratigraphic and well-log sequence-stratigraphic framework for the Scotian Margin, offshore eastern Canada. Canadian Journal of Earth Sciences, v.49(12), pp. 1417-1462.

Withjack, M.O., Schlische, R.W., Olsen, P.E. 1998. Diachronous Rifting, Drifting, and Inversion on the Passive Margin of Central Eastern North America: An Analog for Other Passive Margins. AAPG Bulletin, v. 82, no. 5A, p. 817-835.

Wright, J.D., Miller, K.G., Cramer, B.S., Olsson, R.K., Katz, M.E., Sugarman, P.J. 2001. Transient Climate Events at the Cenomanian/Turonian Boundary (OAE2). American Geophysical Union, Fall Meeting 2001, abstract id. PP32A-0515.

VII. FIGURE CAPTIONS

Figure 1

Map of well data available in Baltimore Canyon Trough. Inset: Basin is outlined in blue, with drilled and plugged wells shown in black.

Figure 2

Seismic profile line 125A from the B-01-75-AT seismic survey, which included the drill site of the COST B2 well. Gamma log data taken from this well is superimposed on the survey, as are traced reflectors used in this study.

Figure 3

Fence diagram of wells from Figure 3 with biostratigraphic event ties between each well. Note the frequent event crossovers and the decreasing of event ties between wells in deeper portions of the section.

Figure 5

Gamma logs for wells COST B2, Exxon 684-1, Texaco 598-1, and Tenneco 642-2. These data rich wells create a dip section (shown on map in red) that is used to assess the relationships of biostratigraphic, lithostratigraphic, sequence, and seismic data. A depth profile of this transect is shown at the top. Prominent sequence boundaries LC1, LC2, LC3, and MISS are traced onto the gamma logs, where the lowest values are white (assuming low GR=quartz sand) and the highest values are black (assuming high GR=mud/shale), to indicate the assumed lithology and aid in the visualization of stacking patterns used to identify major sequences (Miller et al., 2018; Baldwin et al., submitted). Biostratigraphic picks shown in colored dots. Blue circles represent planktonic foraminifera, red circles represent nannofossils, purple circles represent dinoflagellate cysts, green circles represent pollen/spores, and black squares represent OAEs.

Figure 6

ABOVE: Age-depth plots of wells from the dip transect (Figure 5). Top plot shows biostratigraphic events plotted with their total known ranges, with red lines indicating the depth of major sequence boundaries LC1, LC2, LC3, and MISS. The line of correlation (LOC) based on the plotted events is shown in black, with the same sedimentation rate assumed throughout. BELOW: RASC plots of each well using biostratigraphic events with $k \geq 5$. Red line shows the LOC, with blue lines bounding two standard deviations. Note how biostratigraphic events not recorded in the wells are preferentially placed as occurring later than the last plotted event, which skews the overall ranks of these events. A) COST B2 B) Exxon 684-1 C) Tenneco 642-2 D) Texaco 598-1

Figure 7

Events from the Baltimore Canyon Trough composite standard section (BCTCSS) and wells from the analyzed dip transect shown in relationship to the geologic timescale. Hiatuses are shown in gray, with OAEs shown as black bars.

Figure 8

Dendrogram results from the RASC analysis of points with $k \geq 5$, with interevent distances of pairs of biostratigraphic events plotted.

Figure 9

Results of event variance analysis for RASC events. Standard deviations for each taxon used are shown in red and compared to the average standard deviation of variance, shown in black. Note that six taxa have SD higher than the average.

Figure 10

Age-depth plot using the FADs determined by the graphic correlation analysis. Depths are in composite standard units. Biostratigraphic events were selected if they were on or near the LOC. Sequence boundaries are plotted in red, with the LOC shown in black.

Figure 11

Plot of the calculated FAD of all biostratigraphic events used in the graphic correlation. Sequence boundaries plotted in red, with their calculated FAD plotted as large black circles. This plot can be used to identify major hiatuses, including sequence boundaries and prominent maximum flooding surfaces.

Figure 12

Identifying biostratigraphic events of the BCTCSS shown in relationship to major BCT sequences identified by Miller et al. (2018), corresponding facies changes of Schmelz et al. (2019), and depositional environment inferred from these parameters. Major sea level events proposed by Haq (2014) are shown, with events that correlate to hiatuses in BCT highlighted in red.

Figure 13

Range chart of events used in this study, with known ages plotted in solid black bars, and inferred extensions of these ranges plotted as dashed lines. Sequence boundaries are plotted without age, but in superpositional sequence of their occurrence.

Figure 14

ABOVE: A plot similar to figure 10, but with the LOC calculated using a Monte Carlo simulation. Red area shows the iterative regressions, blue lines are biostratigraphic events, and dashed lines encompasses 1.96 SD of all regressions. Ages of major sequence boundaries are shown in colored lines, determined by their calculated FAD and position on the LOC.

BELOW: Sedimentation rates derived from Monte Carlo simulation. Blue shows iterations of the regression, with dashed lines encompassing 95% of the simulations. Black line shows the most likely sedimentation rate calculated by the regressive analyses.

IIIV. FIGURES

Figure 1

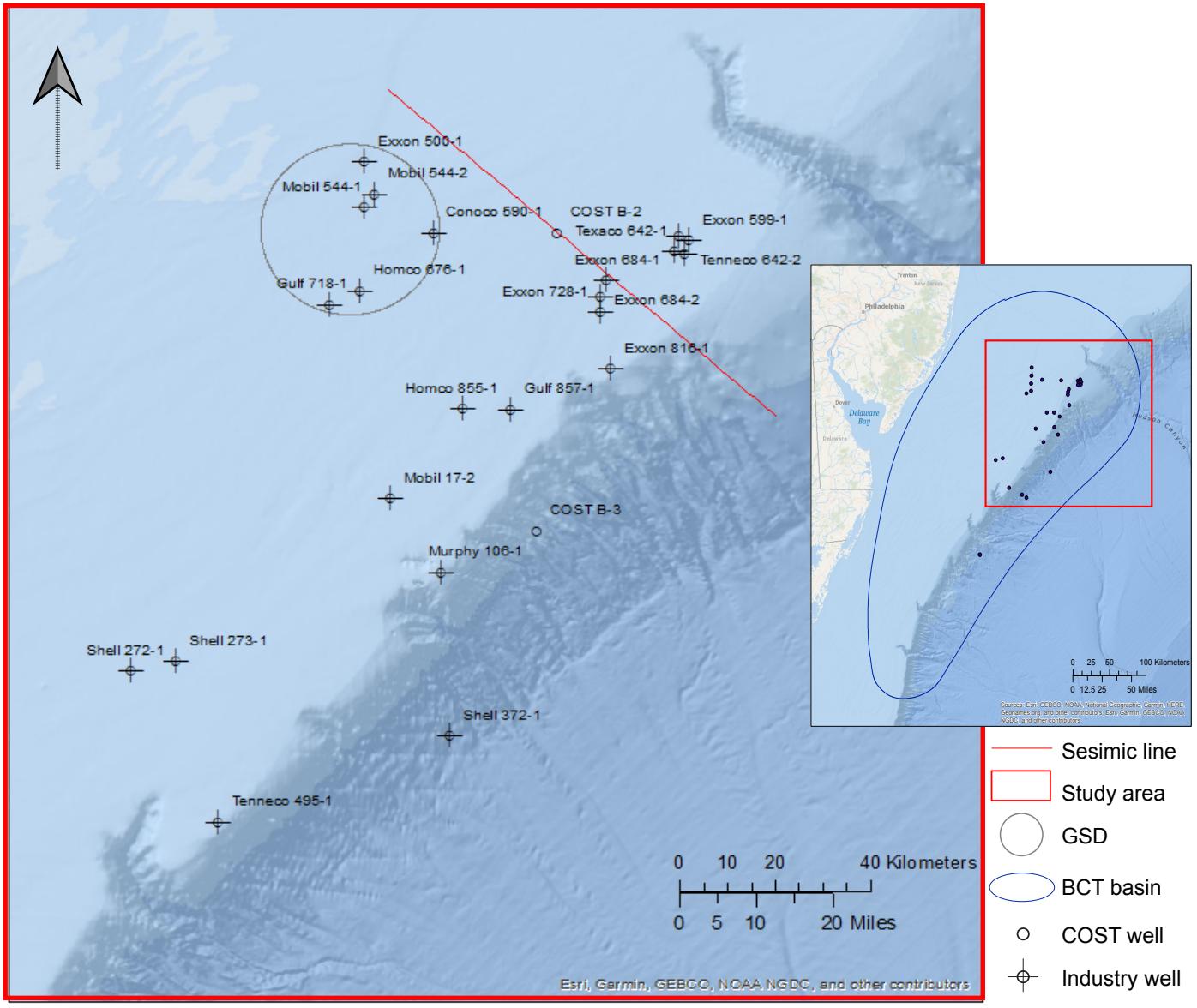

Figure 2

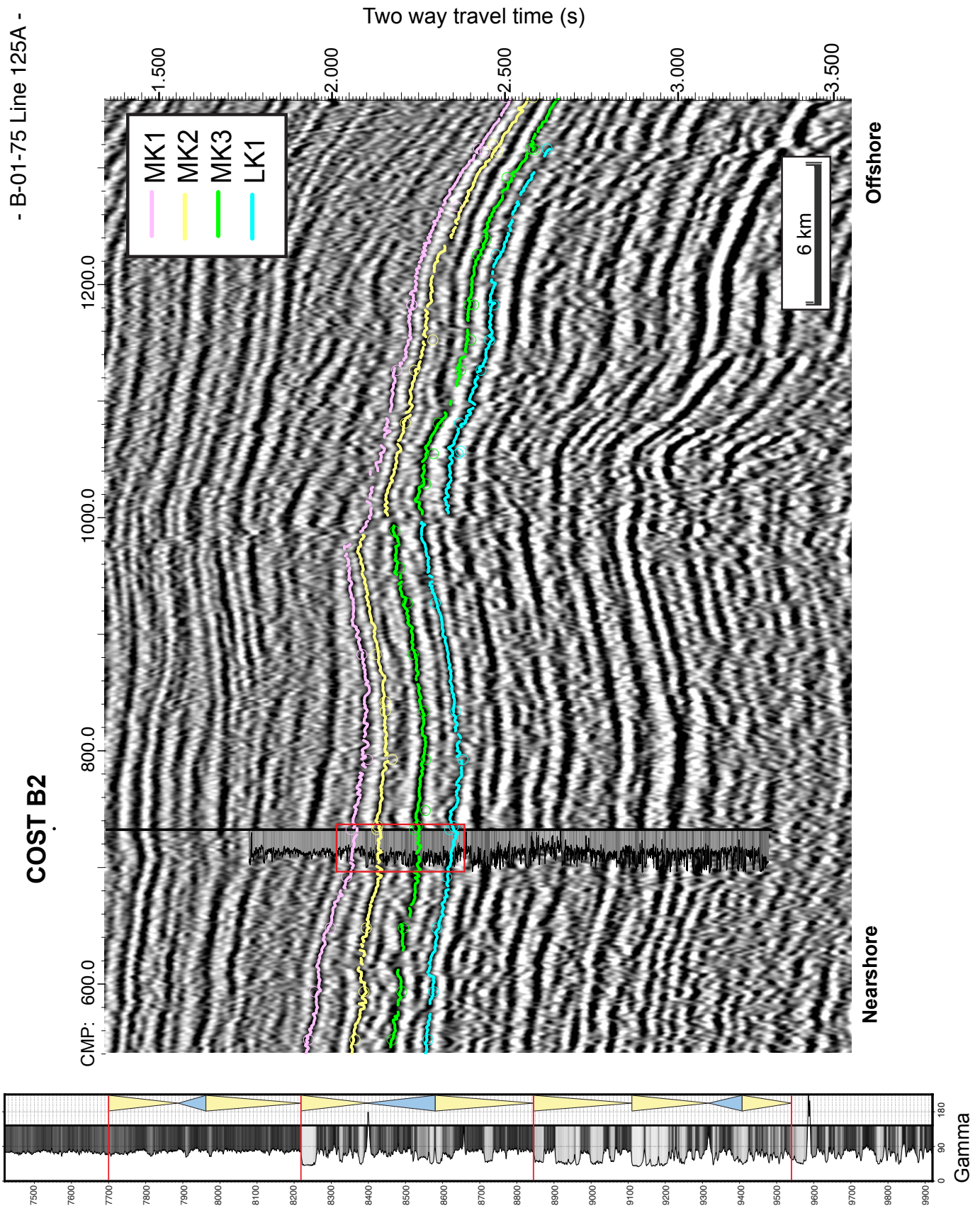
- B-01-75 Line 125A -
COST B2
Two way travel time (s)
1.500
2.000
2.500
3.000
3.500
MK1
MK2
MK3
LK1
6 km
Offshore
Nearshore
CMP:
600.0
800.0
1000.0
1200.0
Gamma
0
90
180
7500
7600
7700
7800
7900
8000
8100
8200
8300
8400
8500
8600
8700
8800
8900
9000
9100
9200
9300
9400
9500
9600
9700
9800
9900

Figure 3

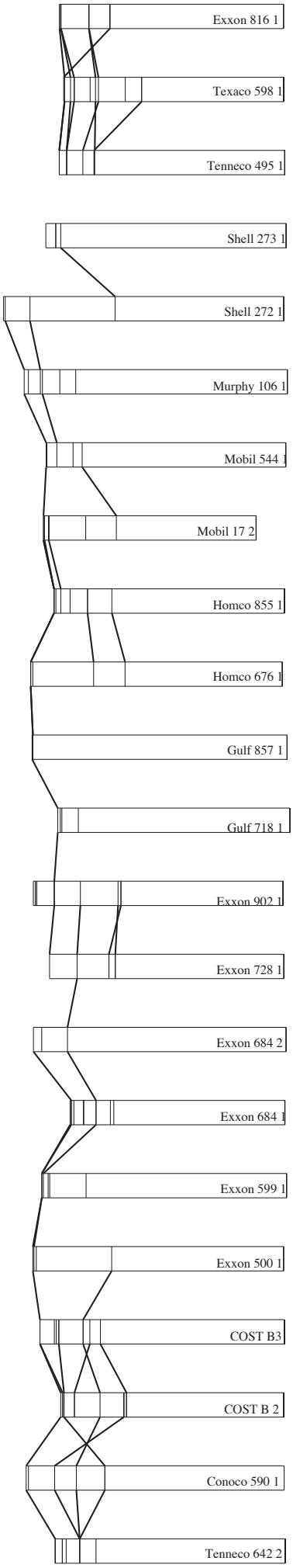
Exxon 816 1
Texaco 598 1
Tenneco 495 1
Shell 273 1
Shell 272 1
Murphy 106 1
Mobil 544 1
Mobil 17 2
Homco 855 1
Homco 676 1
Gulf 857 1
Gulf 718 1
Exxon 902 1
Exxon 728 1
Exxon 684 2
Exxon 684 1
Exxon 599 1
Exxon 500 1
COST B3
COST B 2
Conoco 590 1
Tenneco 642 2

Figure 4

Seismic boundary	Well log sequence	Lithologic Unit	Biostratagraphic markers	Age
MK1	DCx	Dawson Canyon Shale	*Rotalipora cushmani, R. greenhornensis*	Late Cenomanian
MK2	LC1	Logan Canyon 1 Sands	none	Early Cenomanian
MK3	LC2	Logan Canyon 2 Sands	*Braarudosphaera africana*, *Planomalina buxtorfi, Spinidinium vestitum*	Late Albian
LK1	LC3	Logan Canyon 3 Sands	*Cyclonephelium tabulatum*	Late Aptian
LK2	MISS	Missisauga Sandstone	*Aptea anaphrissa, Pseudoceratium pelliferum, Muderongia simplex*	Early Aptian to Barremian

Figure 5

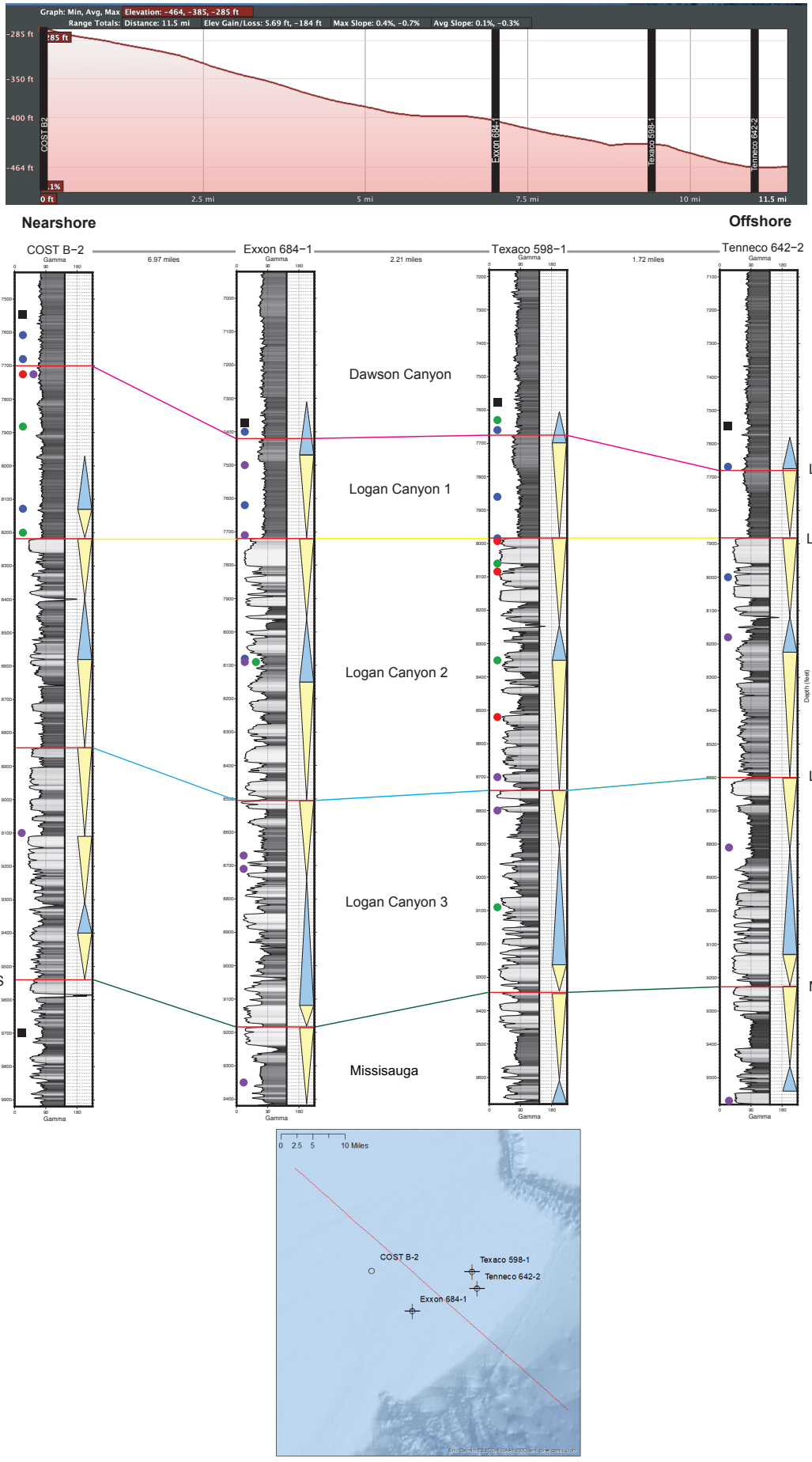
Graph: Min, Avg, Max Elevation: -464, -385, -285 ft
Range Totals: Distance: 11.5 mi Elev Gain/Loss: 5.69 ft, -184 ft Max Slope: 0.4%, -0.7% Avg Slope: 0.1%, -0.3%
-285 ft
-350 ft
-400 ft
-464 ft
COST B2
Exxon 684-1
Texaco 598-1
Tenneco 642-2
0 ft
2.5 mi
5 mi
7.5 mi
10 mi
11.5 mi
Nearshore
Offshore
COST B-2
6.97 miles
Exxon 684-1
2.21 miles
Texaco 598-1
1.72 miles
Tenneco 642-2
Gamma
Depth (feet)
LC1
LC2
LC3
MISS
Dawson Canyon
Logan Canyon 1
Logan Canyon 2
Logan Canyon 3
Missisauga
0 2.5 5 10 Miles
COST B-2
Texaco 598-1
Tenneco 642-2
Exxon 684-1

Figure 6A

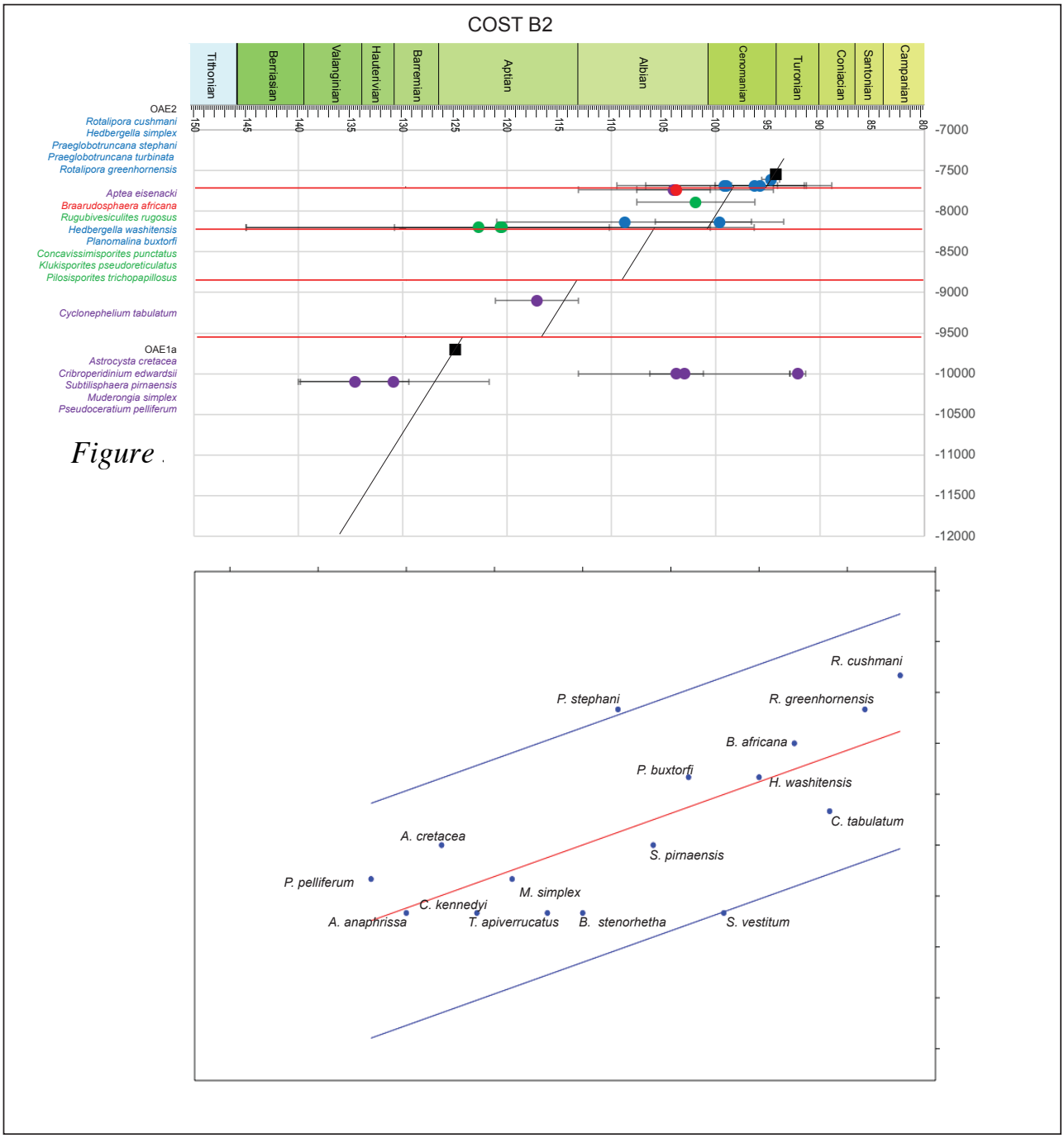

Figure

Figure 6B

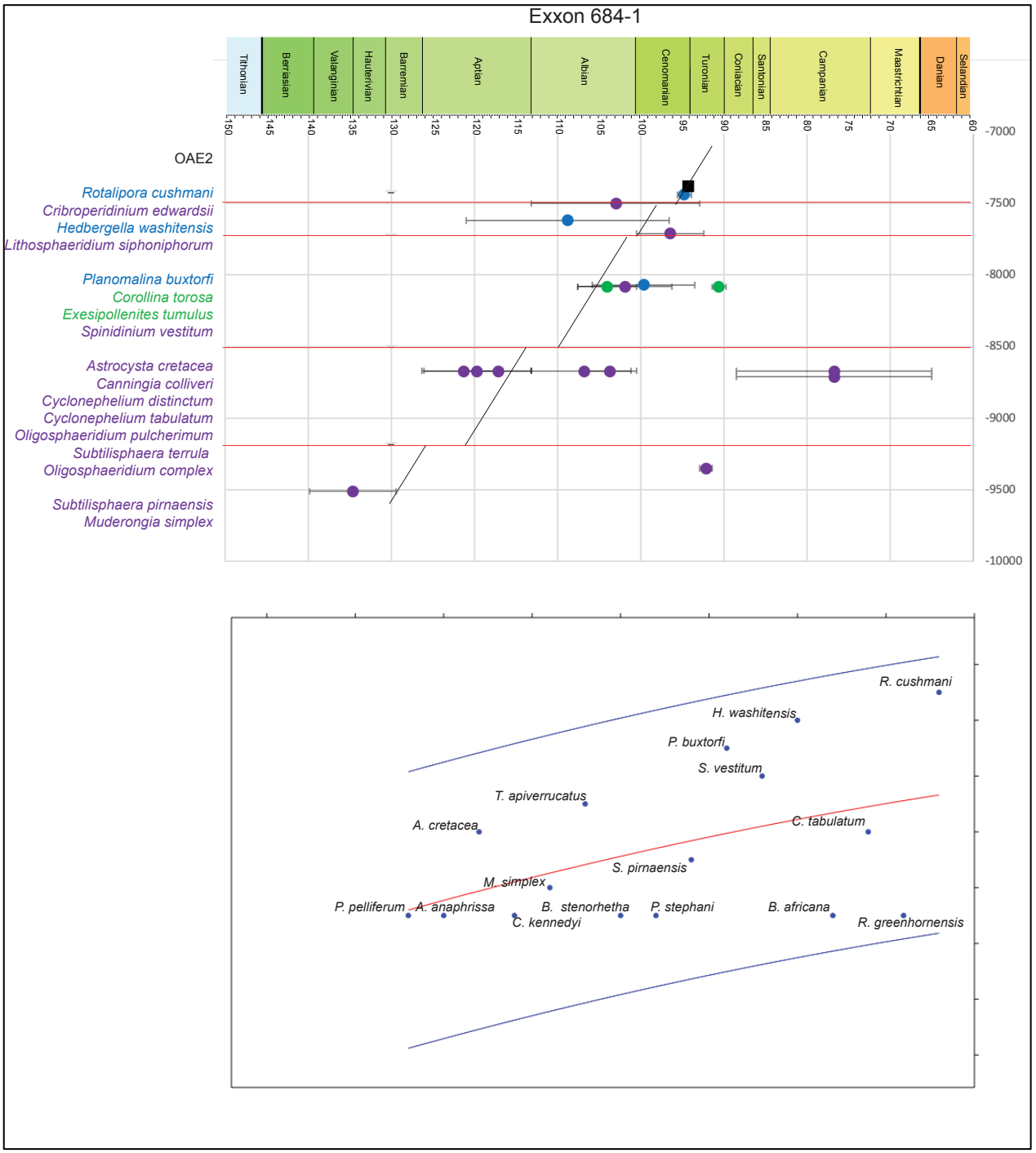
Exxon 684-1
Tithonian
Berriasian
Valanginian
Hauterivian
Barremian
Aptian
Albian
Cenomanian
Turonian
Coniacian
Santonian
Campanian
Maastrichtian
Danian
Selandian
150
145
140
135
130
125
120
115
110
105
100
95
90
85
80
75
70
65
60
-7000
-7500
-8000
-8500
-9000
-9500
-10000
OAE2
Rotalipora cushmani
Cribroperidinium edwardsii
Hedbergella washitensis
Lithosphaeridium siphoniphorum
Planomalina buxtorfi
Corollina torosa
Exesipollenites tumulus
Spinidinium vestitum
Astrocysta cretacea
Canningia colliveri
Cyclonephelium distinctum
Cyclonephelium tabulatum
Oligosphaeridium pulcherimum
Subtilisphaera terrula
Oligosphaeridium complex
Subtilisphaera pirnaensis
Muderongia simplex
R. cushmani
H. washitensis
P. buxtorfi
S. vestitum
T. apiverrucatus
A. cretacea
C. tabulatum
S. pirnaensis
M. simplex
P. pelliferum
A. anaphrissa
B. stenorhetha
C. kennedyi
P. stephani
B. africana
R. greenhornensis

Figure 6C

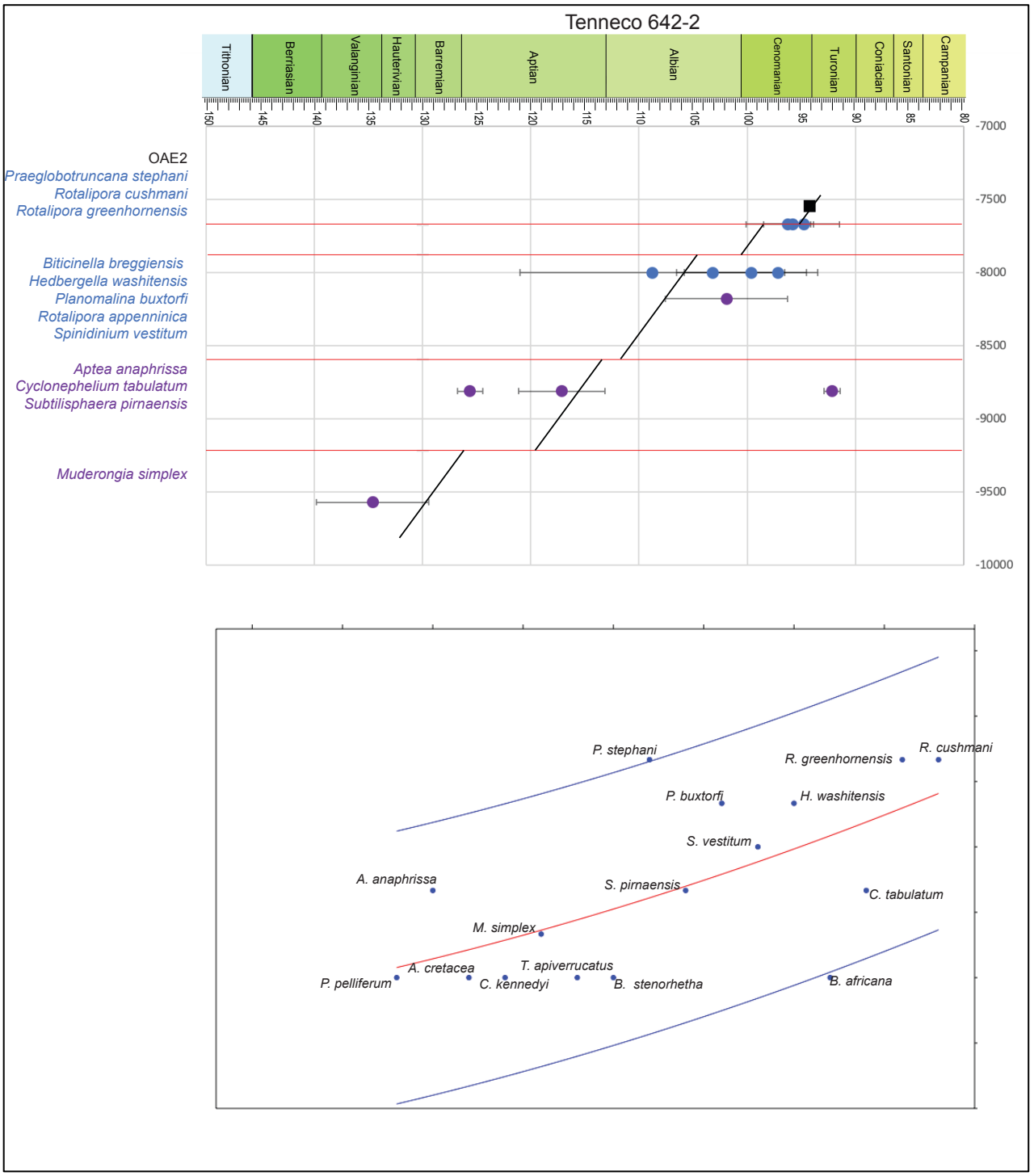
Tenneco 642-2
Tithonian
Berriasian
Valanginian
Hauterivian
Barremian
Aptian
Albian
Cenomanian
Turonian
Coniacian
Santonian
Campanian
150
145
140
135
130
125
120
115
110
105
100
95
90
85
80
-7000
-7500
-8000
-8500
-9000
-9500
-10000
OAE2
Praeglobotruncana stephani
Rotalipora cushmani
Rotalipora greenhornensis
Biticinella breggiensis
Hedbergella washitensis
Planomalina buxtorfi
Rotalipora appenninica
Spinidinium vestitum
Aptea anaphrissa
Cyclonephelium tabulatum
Subtilisphaera pirnaensis
Muderongia simplex
P. stephani
R. greenhornensis
R. cushmani
P. buxtorfi
H. washitensis
S. vestitum
A. anaphrissa
S. pirnaensis
C. tabulatum
M. simplex
A. cretacea
T. apiverrucatus
P. pelliferum
C. kennedyi
B. stenorhetha
B. africana

Figure 6D

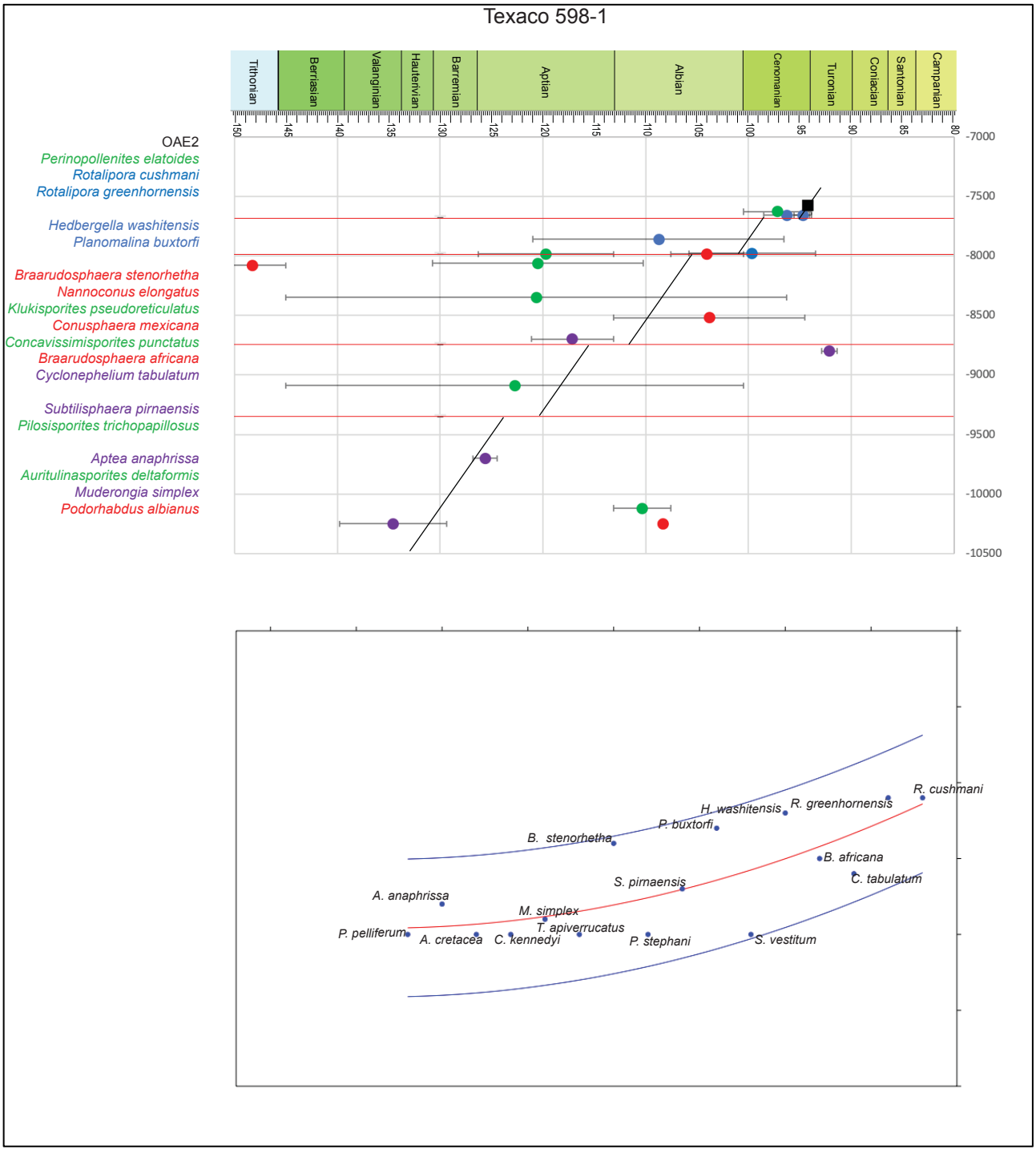
Texaco 598-1
Tithonian
Berriasian
Valanginian
Hauterivian
Barremian
Aptian
Albian
Cenomanian
Turonian
Coniacian
Santonian
Campanian
150
145
140
135
130
125
120
115
110
105
100
95
90
85
80
-7000
-7500
-8000
-8500
-9000
-9500
-10000
-10500
OAE2
Perinopollenites elatoides
Rotalipora cushmani
Rotalipora greenhornensis
Hedbergella washitensis
Planomalina buxtorfi
Braarudosphaera stenorhetha
Nannoconus elongatus
Klukisporites pseudoreticulatus
Conusphaera mexicana
Concavissimisporites punctatus
Braarudosphaera africana
Cyclonephelium tabulatum
Subtilisphaera pirnaensis
Pilosisporites trichopapillosus
Aptea anaphrissa
Auritulinasporites deltaformis
Muderongia simplex
Podorhabdus albianus
R. cushmani
H. washitensis
R. greenhornensis
P. buxtorfi
B. stenorhetha
B. africana
C. tabulatum
S. pirnaensis
A. anaphrissa
M. simplex
T. apiverrucatus
P. pelliferum
A. cretacea
C. kennedyi
P. stephani
S. vestitum

Figure 7

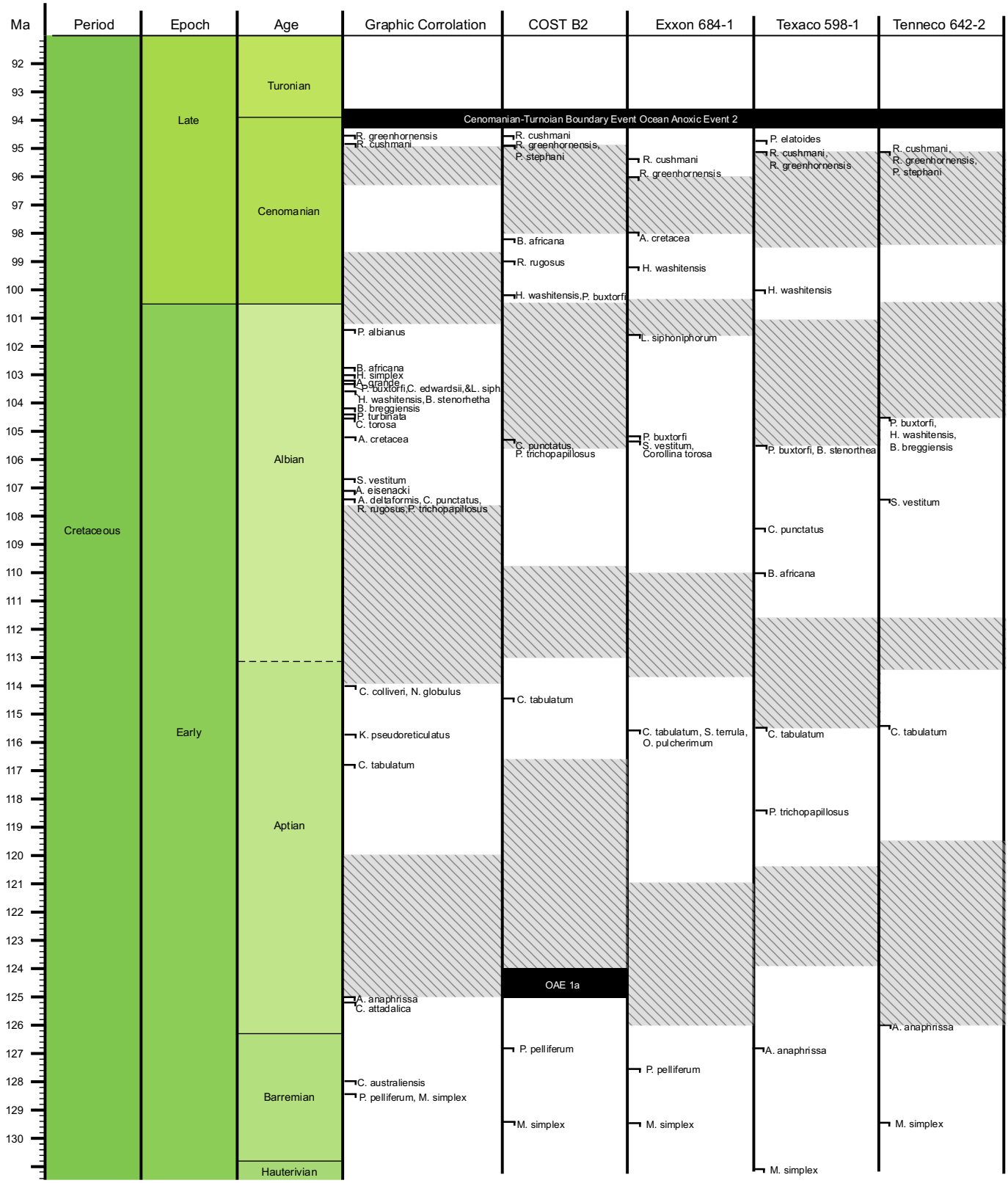
Ma
Period
Epoch
Age
Graphic Corrolation
COST B2
Exxon 684-1
Texaco 598-1
Tenneco 642-2
92
93
94
95
96
97
98
99
100
101
102
103
104
105
106
107
108
109
110
111
112
113
114
115
116
117
118
119
120
121
122
123
124
125
126
127
128
129
130
Cretaceous
Late
Early
Turonian
Cenomanian
Albian
Aptian
Barremian
Hauterivian
Cenomanian-Turnoian Boundary Event Ocean Anoxic Event 2
R. greenhornensis
R. cushmani
P. albianus
B. africana
H. simplex
A. grande
P. buxtorfi,C. edwardsii,&L. siph.
H. washitensis,B. stenorhetha
B. breggiensis
P. turbinata
C. torosa
A. cretacea
S. vestitum
A. eisenacki
A. deltaformis, C. punctatus,
R. rugosus,P. trichopapillosus
C. colliveri, N. globulus
K. pseudoreticulatus
C. tabulatum
A. anaphrissa
C. attadalica
C. australiensis
P. pelliferum, M. simplex
R. cushmani
R. greenhornensis,
P. stephani
B. africana
R. rugosus
H. washitensis,P. buxtorfi
C. punctatus,
P. trichopapillosus
C. tabulatum
OAE 1a
P. pelliferum
M. simplex
R. cushmani
R. greenhornensis
A. cretacea
H. washitensis
L. siphoniphorum
P. buxtorfi
S. vestitum,
Corollina torosa
C. tabulatum, S. terrula,
O. pulcherimum
P. pelliferum
M. simplex
P. elatoides
R. cushmani,
R. greenhornensis
H. washitensis
P. buxtorfi, B. stenorthea
C. punctatus
B. africana
C. tabulatum
P. trichopapillosus
A. anaphrissa
M. simplex
R. cushmani,
R. greenhornensis,
P. stephani
P. buxtorfi,
H. washitensis,
B. breggiensis
S. vestitum
C. tabulatum
A. anaphrissa
M. simplex

Figure 8

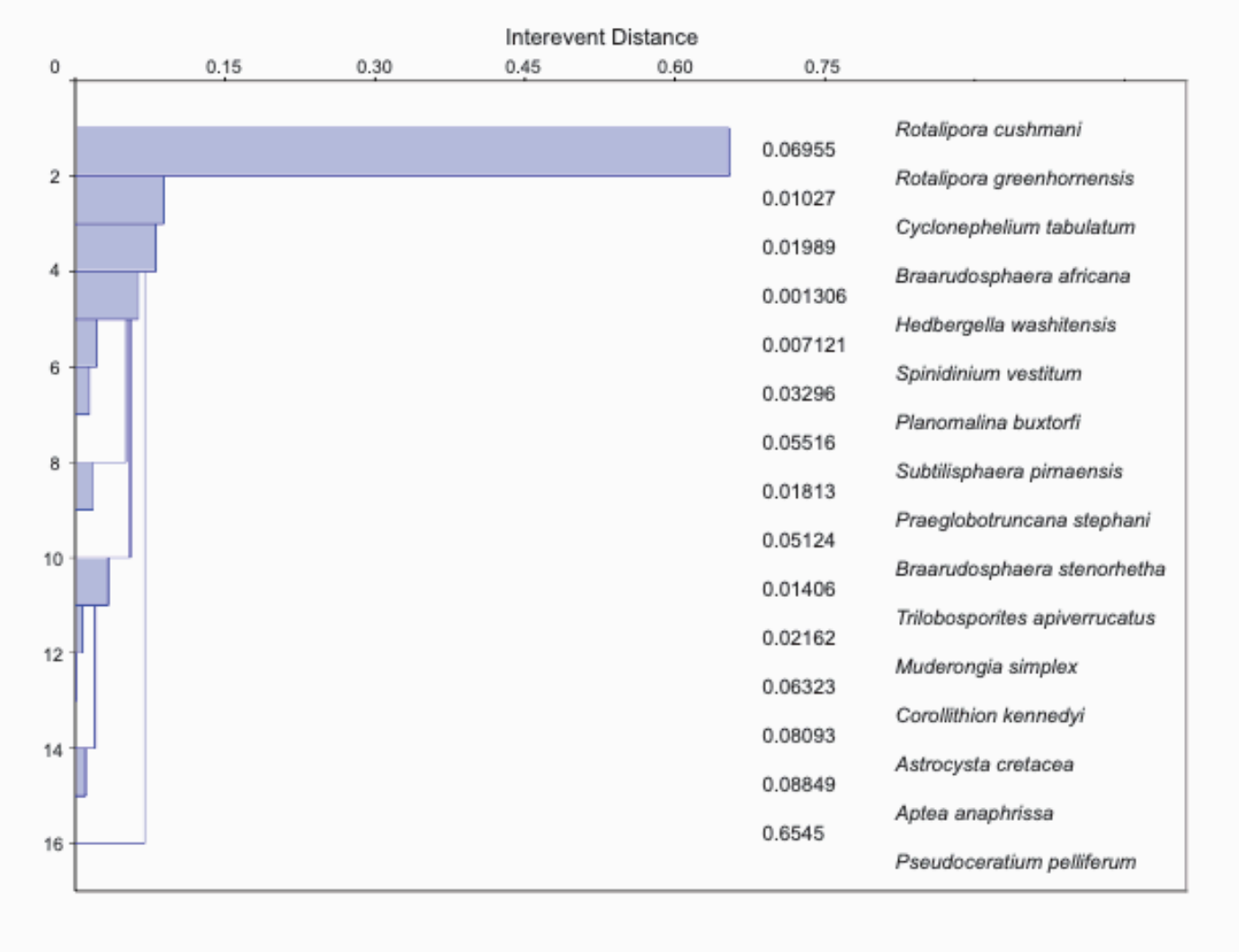
Interevent Distance
0
0.15
0.30
0.45
0.60
0.75
2
4
6
8
10
12
14
16
0.06955
0.01027
0.01989
0.001306
0.007121
0.03296
0.05516
0.01813
0.05124
0.01406
0.02162
0.06323
0.08093
0.08849
0.6545
Rotalipora cushmani
Rotalipora greenhornensis
Cyclonephelium tabulatum
Braarudosphaera africana
Hedbergella washitensis
Spinidinium vestitum
Planomalina buxtorfi
Subtilisphaera pimaensis
Praeglobotruncana stephani
Braarudosphaera stenorhetha
Trilobosporites apiverrucatus
Muderongia simplex
Corollithion kennedyi
Astrocysta cretacea
Aptea anaphrissa
Pseudoceratium pelliferum

Figure 9

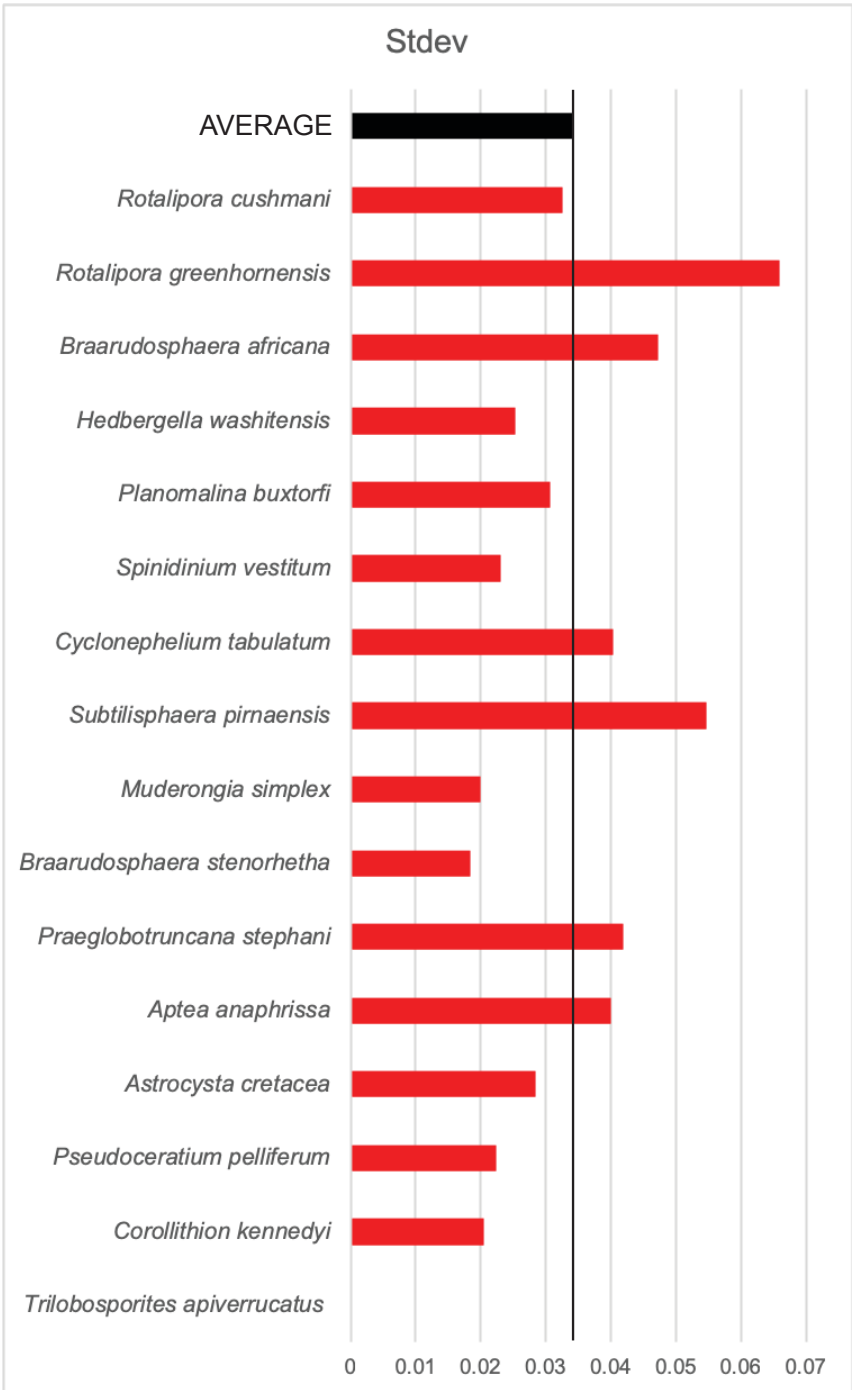
Stdev
AVERAGE
Rotalipora cushmani
Rotalipora greenhornensis
Braarudosphaera africana
Hedbergella washitensis
Planomalina buxtorfi
Spinidinium vestitum
Cyclonephelium tabulatum
Subtilisphaera pirnaensis
Muderongia simplex
Braarudosphaera stenorhetha
Praeglobotruncana stephani
Aptea anaphrissa
Astrocysta cretacea
Pseudoceratium pelliferum
Corollithion kennedyi
Trilobosporites apiverrucatus
0
0.01
0.02
0.03
0.04
0.05
0.06
0.07

Figure 10

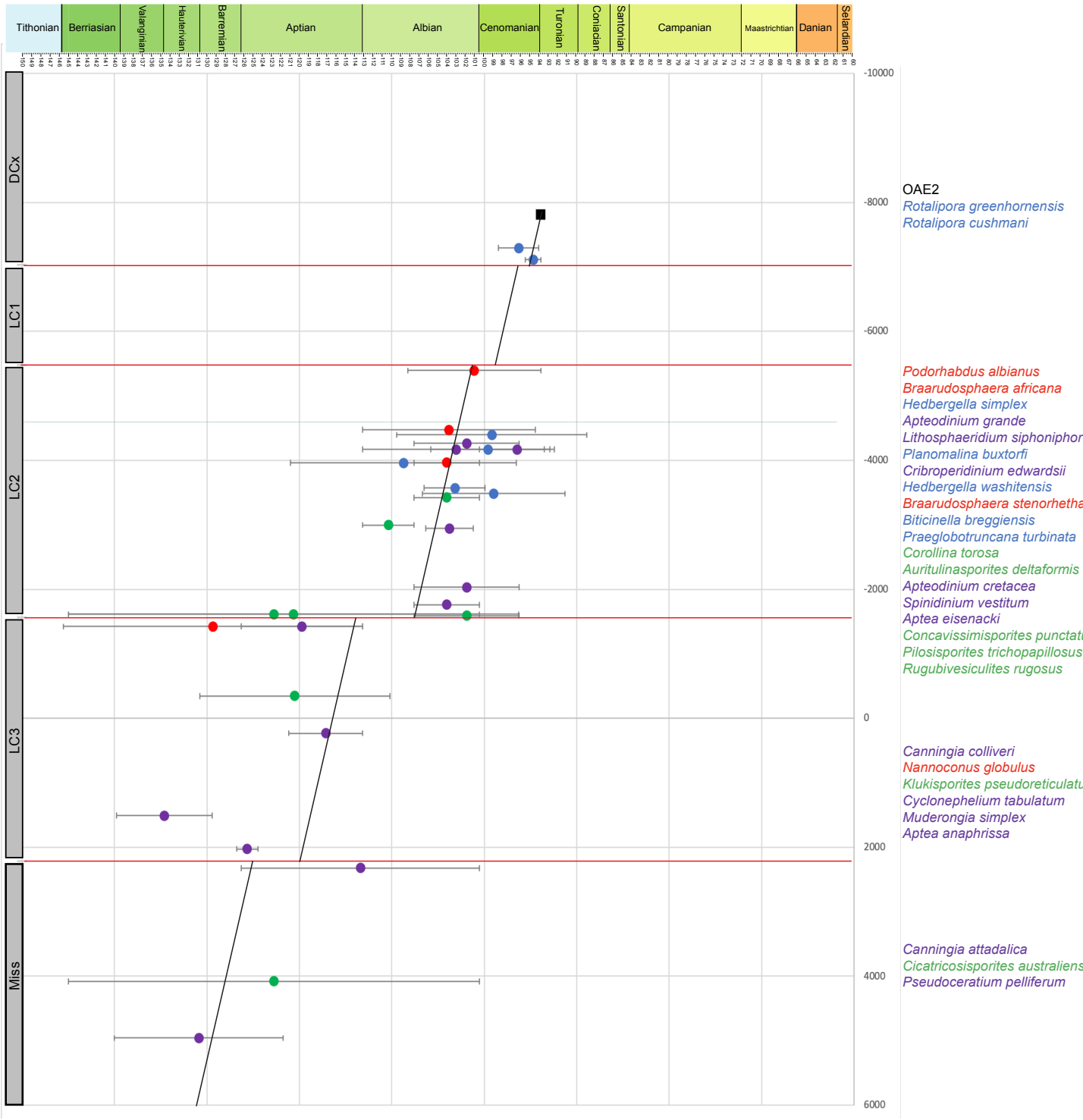
Tithonian
Berriasian
Valanginian
Hauterivian
Barremian
Aptian
Albian
Cenomanian
Turonian
Coniacian
Santonian
Campanian
Maastrichtian
Danian
Selandian
DCx
LC1
LC2
LC3
Miss
-10000
-8000
-6000
-4000
-2000
0
2000
4000
6000
OAE2
Rotalipora greenhornensis
Rotalipora cushmani
Podorhabdus albianus
Braarudosphaera africana
Hedbergella simplex
Apteodinium grande
Lithosphaeridium siphoniphor
Planomalina buxtorfi
Cribroperidinium edwardsii
Hedbergella washitensis
Braarudosphaera stenorhetha
Biticinella breggiensis
Praeglobotruncana turbinata
Corollina torosa
Auritulinasporites deltaformis
Apteodinium cretacea
Spinidinium vestitum
Aptea eisenacki
Concavissimisporites punctat
Pilosisporites trichopapillosus
Rugubivesiculites rugosus
Canningia colliveri
Nannoconus globulus
Klukisporites pseudoreticulatu
Cyclonephelium tabulatum
Muderongia simplex
Aptea anaphrissa
Canningia attadalica
Cicatricosisporites australiens
Pseudoceratium pelliferum

Figure 11

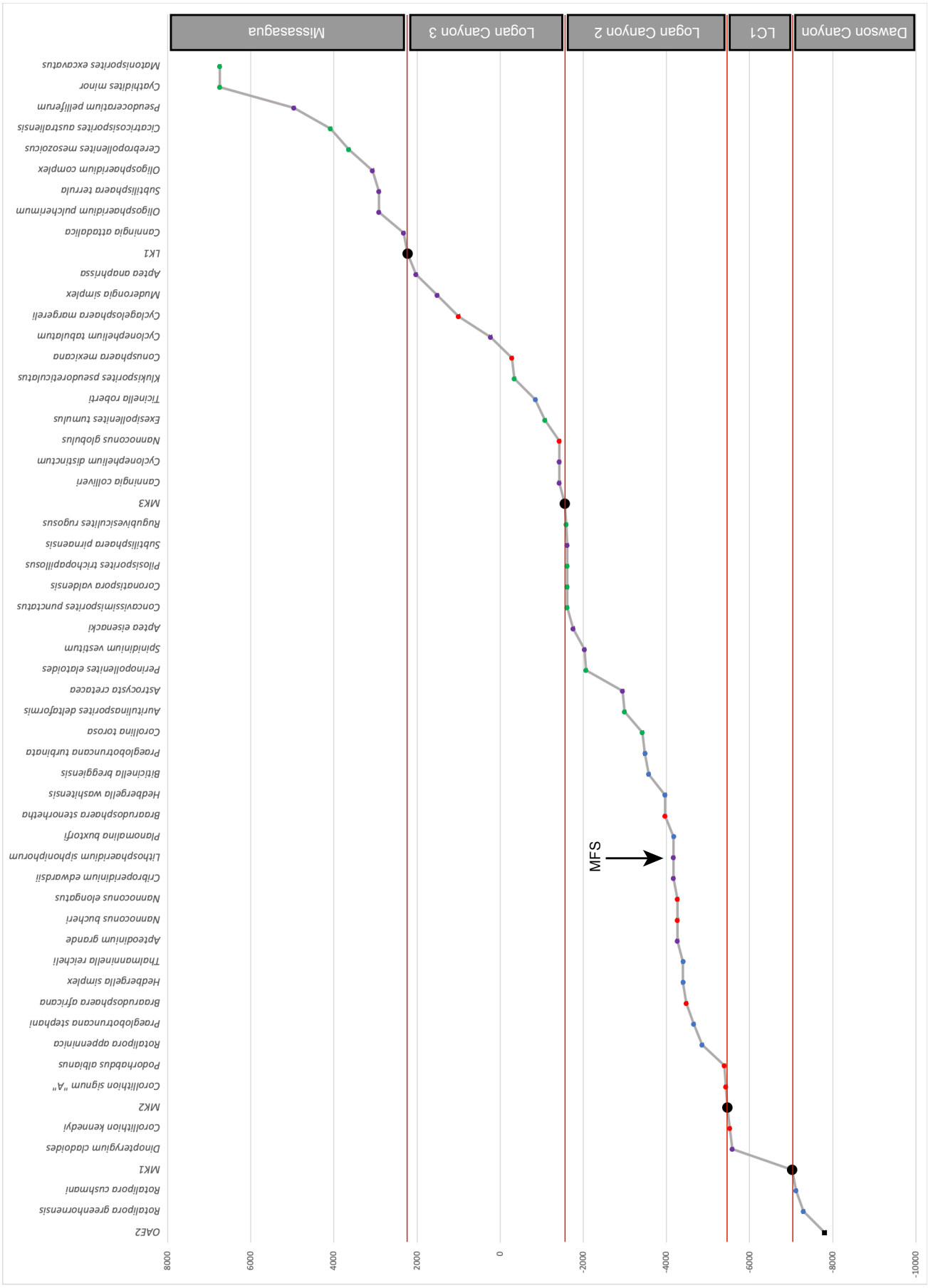
Dawson Canyon
LC1
Logan Canyon 2
Logan Canyon 3
Missasagua
MFS
8000
6000
4000
2000
0
-2000
-4000
-6000
-8000
-10000
OAE2
Rotalipora greenhornensis
Rotalipora cushmani
MK1
Dinopterygium cladoides
Corollithion kennedyi
MK2
Corollithion signum "A"
Podorhabdus albianus
Rotalipora appenninica
Praeglobotruncana stephani
Braarudosphaera africana
Hedbergella simplex
Thalmanninella reicheli
Aptea dinium grande
Nannoconus bucheri
Nannoconus elongatus
Cribroperidinium edwardsii
Lithosphaeridium siphoniphorum
Planomalina buxtorfi
Braarudosphaera stenorhetha
Hedbergella washitensis
Bitticinella breggiensis
Praeglobotruncana turbinata
Corollina torosa
Aurtulinasporites deltaformis
Astrocysta cretacea
Perinopollenites elatoides
Spinidinium vestitum
Aptea eisenacki
Concavissimisporites punctatus
Coronatispora valdensis
Pilosisporites trichoppapillosus
Subtilisphaera pirnaensis
Rugubivesiculites rugosus
MK3
Canningia colliveri
Cycloneph elium distinctum
Nannoconus globulus
Exesipollenites tumulus
Ticinella roberti
Klukisporites pseudoreticulatus
Conusphaera mexicana
Cycloneph elium tabulatum
Cyclageloshaera margerelli
Muderonglia simplex
Aptea anaphrissa
LK1
Canningia attadalica
Oligosphaeridium pulcherimum
Subtilisphaera terrula
Oligosphaeridium complex
Cerebropollenites mesozoicus
Cicatricosisporites australiensis
Pseudoceratium pelliferum
Cyathidites minor
Matonisporites excavatus

Figure 12

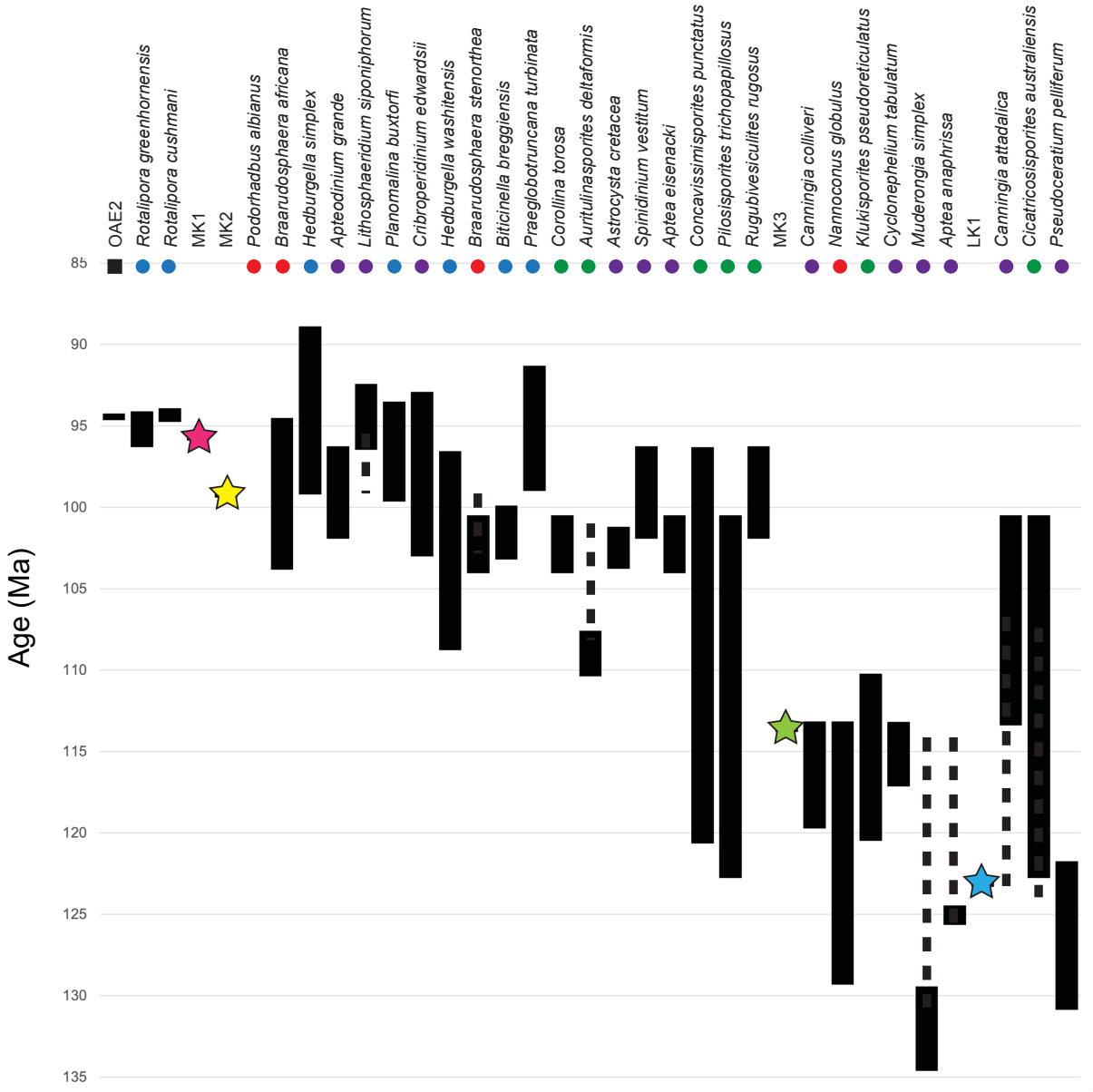
OAE2
Rotalipora greenhornensis
Rotalipora cushmani
MK1
MK2
Podorhabdus albianus
Braarudosphaera africana
Hedburgella simplex
Apteodinium grande
Lithosphaeridium siponiphorum
Planomalina buxtorfi
Cribroperidinium edwardsii
Hedburgella washitensis
Braarudosphaera stenorthea
Biticinella breggiensis
Praeglobotruncana turbinata
Corollina torosa
Auritulinasporites deltaformis
Astrocysta cretacea
Spinidinium vestitum
Aptea eisenacki
Concavissimisporites punctatus
Pilosisporites trichopapillosus
Rugubivesiculites rugosus
MK3
Canningia colliveri
Nannoconus globulus
Klukisporites pseudoreticulatus
Cyclonephelium tabulatum
Muderongia simplex
Aptea anaphrissa
LK1
Canningia attadalica
Cicatricosisporites australiensis
Pseudoceratium pelliferum
Age (Ma)
85
90
95
100
105
110
115
120
125
130
135

Figure 13

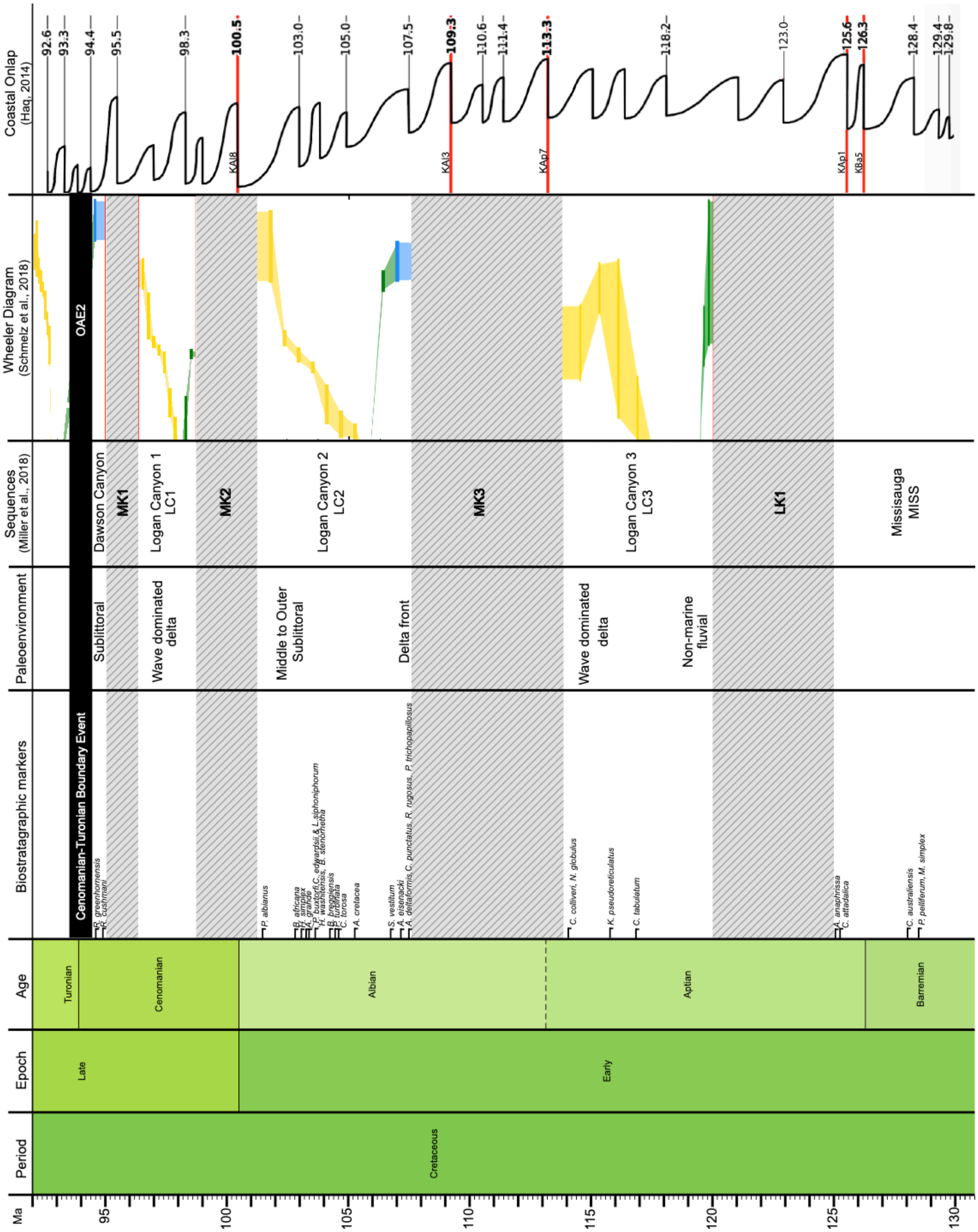
Coastal Onlap (Haq, 2014)
Wheeler Diagram (Schmelz et al., 2018)
Sequences (Miller et al., 2018)
Paleoenvironment
Biostratagraphic markers
Age
Epoch
Period
Ma
OAE2
Cenomanian-Turonian Boundary Event
Dawson Canyon
MK1
Logan Canyon 1 LC1
MK2
Logan Canyon 2 LC2
MK3
Logan Canyon 3 LC3
LK1
Missisauga MISS
Sublittoral
Wave dominated delta
Middle to Outer Sublittoral
Delta front
Non-marine fluvial
Turonian
Cenomanian
Albian
Aptian
Barremian
Late
Early
Cretaceous
KAl8
KAl3
KAp7
KAp1
KBa5
92.6
93.3
94.4
95.5
98.3
100.5
103.0
105.0
107.5
109.3
110.6
111.4
113.3
118.2
123.0
125.6
126.3
128.4
129.4
129.8
95
100
105
110
115
120
125
130

Figure 14

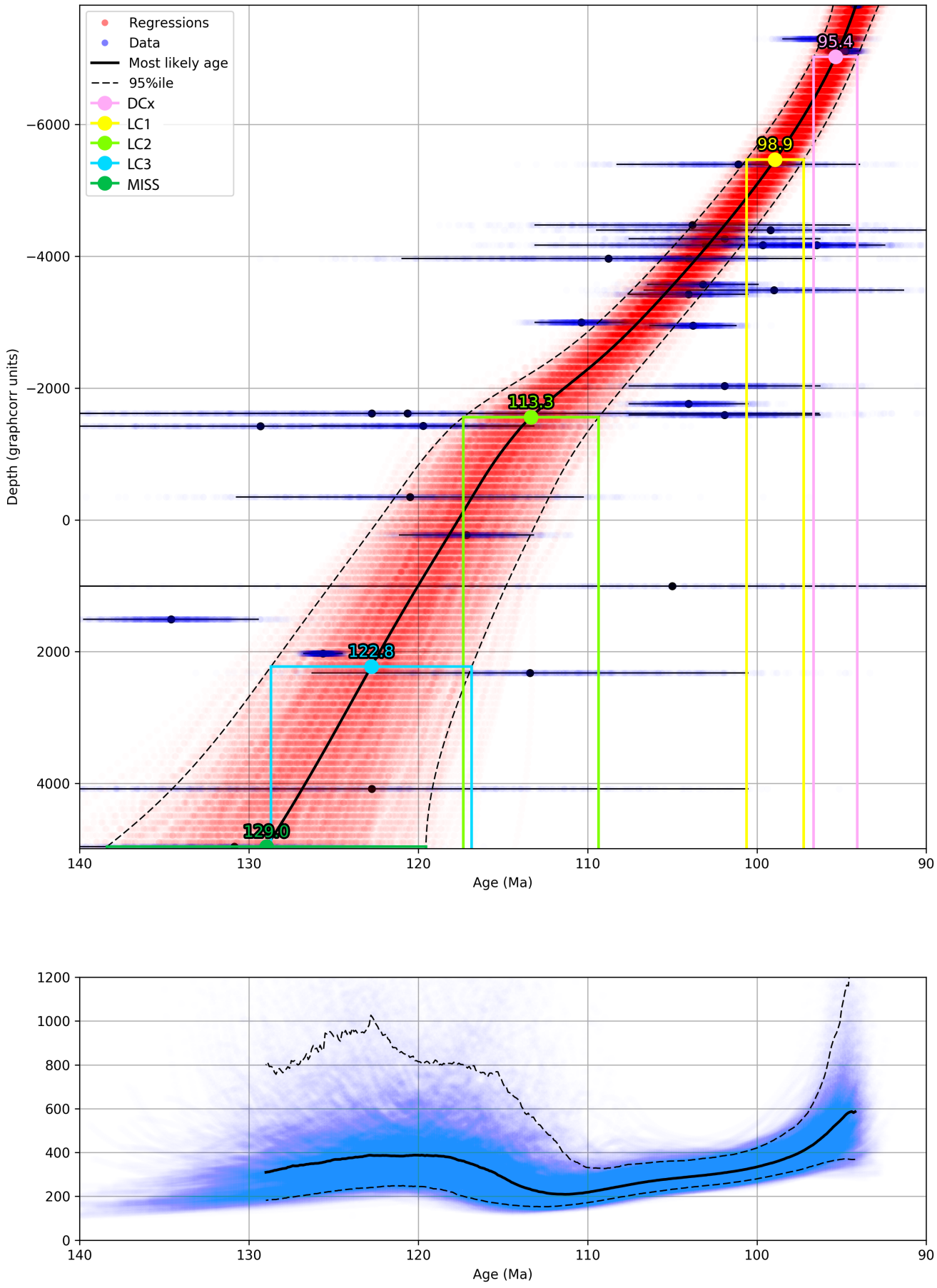
Regressions
Data
Most likely age
95%ile
DCx
LC1
LC2
LC3
MISS
95.4
98.9
113.3
122.8
129.0
Depth (graphcorr units)
−6000
−4000
−2000
0
2000
4000
140
130
120
110
100
90
Age (Ma)
1200
1000
800
600
400
200
0
140
130
120
110
100
90
Age (Ma)

VIII. APPENDICES

i. Appendix A

Highest and lowest occurrences for taxa used in quantitative analyses of this study.

Species	Group	HO	LO	Reference
Aptea anaphrissa	Dinoflagellate	124.46	126.8	Hardenbol et al., 1998
Aptea eisenacki	Dinoflagellate	100.5	107.59	Williams et al., 2017
Apteodinium grande	Dinoflagellate	96.24	107.59	Williams et al., 2017
Astrocysta cretacea	Dinoflagellate	101.19	106.35	Hardenbol et al., 1998
Auritulinasporites deltaformis	Pollen/spore	107.59	113.14	Broatch 1987
Biticinella breggiensis	Foraminifera	99.9	106.5	Ogg et al., 2016
Braarudosphaera africana	Nannofossil	94.5	113.14	Ogg et al., 2016
Braarudosphaera stenorhetha	Nannofossil	100.5	107.59	Young et al., 2017
Canningia attadalica	Dinoflagellate	100.5	126.3	Williams et al., 2017
Canningia colliveri	Dinoflagellate	113.14	126.3	Williams et al., 2017
Cerebropollenites mesozoicus	Pollen/spore	100.5	113.14	Brideaux, 1968
Cicatricosisporites australiensis	Pollen/spore	100.5	145	Brenner, 1962
Concavissimisporites punctatus	Pollen/spore	96.29	145	Bebout, 1981
Conusphaera mexicana	Nannofossil	145.01	151.5	Young et al., 2017
Corollina torosa	Pollen/spore	100.5	107.59	Steinkraus, 1979
Corollithion kennedyi	Nannofossil	94.1	95.92	Ogg et al., 2016
Corollithion signum "A"	Nannofossil	65	100.5	Young et al., 2017
Coronatispora valdensis	Pollen/spore	93.9	100.5	Cousminer, 1986
Cribroperidinium edwardsii	Dinoflagellate	92.9	113.14	Williams et al., 2017
Cyathidites minor	Pollen/spore	65	88.45	Gray and Groot, 1966
Cyclagelosphaera margerelli	Nannofossil	65	145	Young et al., 2017
Cyclonephelium distinctum	Dinoflagellate	65	88.45	Williams et al., 2017
Cyclonephelium tabulatum	Dinoflagellate	113.16	121.14	Ogg et al., 2016

Dinopterygium cladoides	Dinoflagellate	65	88.45	Ogg et al., 2016
Exesipollenites tumulus	Pollen/spore	89.75	91.39	Steinkraus, 1979
Hedbergella simplex	Foraminifera	88.9	109.5	Blow, 1979.
Hedbergella washitensis	Foraminifera	96.55	121	Boudagher et al., 1997
Klukisporites pseudoreticulatus	Pollen/spore	110.22	130.77	Scott et al., 1977
Litosphaeridium siphoniphorum	Dinoflagellate	92.43	100.5	Hardenbol et al., 1998
Matonisporites excavatus	Pollen/spore	93.9	100.5	Kimyai, 1964
Muderongia simplex	Dinoflagellate	129.41	139.8	Ogg et al., 2016
Nannoconus bucheri	Nannofossil	113.14	132.9	Ogg et al., 2016
Nannoconus elongatus	Nannofossil	113.14	126.3	Young et al., 2017
Nannoconus globulus	Nannofossil	113.14	145.5	Young et al., 2017
Nannoconus steinmannii	Nannofossil	113.16	145.5	Ogg et al., 2016
Oligosphaeridium complex	Dinoflagellate	65	88.45	Williams et al., 2017
Oligosphaeridium pulcherimum	Dinoflagellate	100.5	113.14	Williams et al., 2017
Perinopollenites elatoides	Pollen/spore	93.9	100.5	Steinkraus, 1979
Pilosisporites trichopapillosus	Pollen/spore	100.5	145	Brenner, 1962
Planomalina buxtorfi	Foraminifera	93.5	105.8	Ogg et al., 2016
Podorhabdus albianus	Nannofossil	93.9	108.3	Ogg et al., 2016
Praeglobotruncana stephani	Foraminifera	91.5	100.1	Robaszynski and Carson, 1982
Praeglobotruncana turbinata	Foraminifera	91.3	106.7	Boudagher-Fadel, 2015
Pseudoceratium pelliferum	Dinoflagellate	121.74	140	Ogg et al., 2016
Rotalipora appenninica	Foraminifera	94.5	99.8	Ogg et al., 2016
Rotalipora cushmani	Foraminifera	93.9	95.6	Ogg et al., 2016
Rotalipora greenhornensis	Foraminifera	94.1	98.5	Ogg et al., 2016
Rugubivesiculites rugosus	Pollen/spore	96.24	107.59	Robbins et al., 1975
Spinidinium vestitum	Dinoflagellate	96.24	107.59	Williams et al., 2017
Subtilisphaera pirnaensis	Dinoflagellate	91.39	92.9	Williams et al., 2017
Subtilisphaera terrula	Dinoflagellate	116.58	126.08	Ogg et al., 2016
Thalmanninella reicheli	Foraminifera	95.4	95.8	Ogg et al., 2016
Ticinella roberti	Foraminifera	100.4	104.42	Leckie et al., 2002

SUPPLEMENTARY REFERENCES

Bebout, J.W. 1981. An informal palynologic zonation for the Cretaceous System of the United States Mid-Atlantic, (Baltimore Canon Area), Outer Continental Shelf. Palynology, v. 5, pp. 159-194.

Blow, W.H. 1979. The Cainozoic Globigerinida. Leiden, Netherlands: E.J.Brill; p. 1413.

Boudagher, M.K., Banner, F.T., Whittaker, J.E. 1997. The Early evolutionary history of planktonic foraminifera. London: Chapman & Hall. 288 p.

Boudagher-Fadel, M.K. 2015. Biostratigraphic and geologic significance of planktonic foraminifera. UCL Press, 306 pp.

Brenner, G.J. 1962. The spores and pollen of the Potomac Group of Maryland. PhD Thesis, Pennsylvania State University.

Brenner, G.J. 1963. The spores and pollen of the Potomac Group of Maryland. Maryland Geological Survey, Bulletin no. 27, 215 pp.

Brideaux, W.W. 1968. Palynology of the Lower Colorado Group (Late Lower Cretaceous) and its lithological equivalents in central and west-central Alberta, Canada. PhD Thesis, McMaster University.

Broatch, J.C.1987. Palynological zonation and correlation of the Peace River Coalfield northeastern British Columbia: An update. MS thesis, University of British Columbia.

Cousminer, H.L. 1986. "Biostratigraphy", Shell Wilmington Canyon 586-1 Well, Geological and Operational Summary. G.M. Edson, editor.

Gonzales-Donoso, J.M., Linares, D., Robaszynski, F. 2007. The rotaliporids, a polyphyletic group of Albian Cenomanian planktonic foraminifera: emendation of genera. Journal of Foraminiferal Research, v. 37(2), pp. 175-186.

Gray, T.C. and Groot, J.J. 1966. Pollen and spores from the marine Upper Cretaceous formations of Delaware and New Jersey. Palentolographica B, v. 117, pp. 114-134, pls. 42-43.

Hardenbol, J., Thierry, J., Farley, M.B., Jacquin, T., de Graciansky, P.C. and Vail, P. 1998. Mesozoic and Cenozoic Sequence Chronostratigraphic Framework of European Basins. In: De Graciansky, P.C., et al., Eds., Mesozoic and Cenozoic Sequence Stratigraphy of European Basins, 60, charts 1-8, SEPM Special Publication, pp. 3-13.

Kimyai, A. 1964. Plant microfossils from the Raritan Formation (Cretaceous) in Long Island. MS thesis, New York University.

Leckie, R.M., Bralower, T.J., Cashman, R. 2002. Oceanic anoxic events and plankton evolution: biotic response to tectonic forcing during the mid-Cretaceous. Paleoceanography, v.17(3): pp. 129.

Lipson-Benitah, S. 2008. Phylogeny of the Middle Cretaceous (Late Albian-Late Cenomanian) planktonic foraminiferal genera *Parathalmanninella* nov. gen. and *Thalmanninella*. Journal of Foraminiferal Research, v.38(2), pp. 183-219.

Ogg, J.G., Ogg, G.M., Gradstein, F.M. 2016. A Concise Geologic Timescale. Elsevier, 240 pp.

Robaszynski F., Caron M. 1982. #Atlas de Foraminiferes Planctoniques du Cretace Moyen (Mer Boreale et Tethys). Paris: Cahiers de Micropaleontologie, v. 1, p. 1185.

Robbins, E.I., Perry, W.J., Doyle, J.A. 1975. Palynological and stratigraphic investigations of four deep wells in the Salisbury Embayment of the Atlantic Coastal Plain. U.S. Geological Open File Report 75-307, 120 p.

Scott, R.A. 1977. "Palynomorph biostratigraphy", Geological studies on the COST No. B-2 well, U.S. Mid-Atlantic outer continental shelf, Circular 750. Scholle, P.A. ed., U.S. Geological Survey 10.3133/cir750.

Steinkraus, W.E. 1979. "Biostratigraphy". Geological and Operational summary, Cost No.B-3 Well, Baltimore Canyon Trough area, Mid-Atlantic OCS. R.V. Amato and E.K. Simonis, eds. United States Geological Survey, Open-File Report Vol. 79 # 1159 P. 21- 31

Williams, G.L., Fensome, R.A., and MacRae, R.A., 2017. DINOFLAJ3. American Association of Stratigraphic Palynologists, Data Series no. 2.

Young, J.R., Brown P.R., Lees J.A. 2017. Nannotax3 website. International Nannoplankton Association.

ii. Appendix B

Synonymized taxonomy used in well reports for this study.

EVENT	Author	Synonym
Aptea anaphrissa	Sarjeant, 1966	*Tenua anaphrissa* Benedek, 1972
Aptea eisenackii	Davey 1969	
Apteodinium grande	Cookson and Hughes, 1964	
Astrocysta cretacea	Pocock, 1962	*Palaeoperidinium cretaceum* Pocock, 1962
Auritulinasporites deltaformis	Burger, 1966	
Biticinella breggiensis	Gandolfi, 1942	
Braarudosphaera africana	Stradner, 1961	
Braarudosphaera stenorhetha	Hill, 1976	
Canningia attadalica	Cookson and Eisenack, 1962	*Cyclonephelium attadalicum*
Canningia colliveri	Cookson and Eisenack, 1960	
Cerebropollenites mesozoicus	Nilsson, 1958	
Cicatricosisporites australiensis	Cookson, 1956	Potonie and Gelletich, 1961
Concavissimisporites punctatus	Delcourt and Sprumont, 1955	
Conusphaera mexicana	Trejo, 1969	
Corollina torosa	Reissinger, 1977	*Classopollis classoides* Pflug, 1964 *Corolina torosus* Reissinger, 1957
Corollithion kennedyi	Crux, 1981	
Corollithion signum "A"	Stradner, 1963	
Cribroperidinium edwardsii	Cookson and Eisenack, 1958	
Cyathidites minor	Couper, 1953	
Cyclagelosphaera margerelli	Noël, 1965	
Cyclonephelium distinctum	Deflandre and Cookson, 1955	
Cyclonephelium tabulatum	Davey and Verdier, 1974	*Aptea dampieri* Balme, 1957
Dinopterygium cladoides	Deflandre, 1935	
Exesipollenites tumulus	Balme 1957	
Hedbergella simplex	Gasinski, 1988	*Clavihedbergella simplex* Morrow, 1934
Hedbergella washitensis	Carsey, 1926	*Favusella washitensis* Carsey, 1926
Klukisporites pseudoreticulatus	Couper, 1958	
Litosphaeridium siphoniphorum	Cookson and Eisenack, 1958	
Matonisporites excavatus	Brenner, 1963	
Muderongia simplex	Alberti, 1961	

Nannoconus bucheri	Brönnimann, 1955	
Nannoconus elongatus	Brönnimann, 1955	
Nannoconus globulus	Brönnimann, 1955	
Oligosphaeridium complex	Davey and Williams, 1966	
Oligosphaeridium pulcherrimum	Davey and Williams, 1966	
Perinopollenites elatoides	Couper, 1958	
Pilosisporites trichopapillosus	Delcourt and Sprumont, 1955	
Planomalina buxtorfi	Gandolfi, 1942	
Podorhabdus albianus	Black, 1967	*Podorhabdus orbiculofenestrus* Gartner, 1968
Praeglobotruncana stephani	Gandolfi, 1942	
Praeglobotruncana turbinata	Reichel, 1950	
Pseudoceratium pelliferum	Gocht, 1957	
Rotalipora appenninica	Renz, 1936	
Rotalipora cushmani	Morrow, 1934	
Rotalipora greenhornensis	Morrow, 1934	
Rugubivesiculites rugosus	Pierce, 1961	
Spinidinium vestitum	Brideaux, 1971	
Subtilisphaera pirnaensis	Alberti, 1959	*Deflandrea pirnaensis*
Subtilisphaera terrula	Davey, 1974	
Thalmanninella reicheli	Mornod, 1950	*Rotalipora reicheli*
Ticinella roberti	Gandolfi, 1942	